This project has received funding from the European Union's Horizon 2020 Programme

SAMPLEIV [EASA.2020.FC05]

[DELIVERABLE 1: REPORT]

DATA REPORT: Potential Improvements to Current ICAO nvPM Sampling & Measurement System

An Agency of the European Union

Disclaimer

Funded by the European Union. Views and opinions expressed are however those of the author(s) only and do not necessarily reflect those of the European Union or the European Union Aviation Safety Agency (EASA). Neither the European Union nor EASA can be held responsible for them.

DELIVERABLE NUMBER AND TITLE: [SAMPLEIV, D1]
CONTRACT NUMBER: EASA.2020.FC05
CONTRACTOR / AUTHOR: Dr's M. Johnson (RR), A Crayford (CU), E. Durand (CU), P. Williams (UoM), L. Durdina (ZHAW) and G. Smallwood (NRC Canada)
IPR OWNER: European Union Aviation Safety Agency
DISTRIBUTION: Public

REVIEWED AND SIGNED OFF BY			
ROLE	DATE	NAME	SIGNATURE
LEAD AUTHOR	8th November 2024	Mark Johnson	
LEAD AUTHOR & TECHNICAL LEAD	11th November 2024	Andrew Crayford	

EXECUTIVE SUMMARY

To understand potential improvements that could be made to the current ICAO Annex 16 vol. II nvPM sampling and measurement standards and system loss correction reporting, as part of the SAMPLE IV project, a series of experiments were designed and conducted at both Cardiff University's Gas Turbine Research Centre (GTRC) and Rolls-Royce Derby in 2021/2022. In consultation with EASA and the relevant SAE E31 teams and sub-committees, several specific independent experiments were performed to assess:

1. A reported issue of unquantified thermophoretic loss uncertainty resulting from adverse temperature gradients and compliance with respect to ensuring a 145 °C minimum temperature at T_1 in the dilution box (Module 2 - as defined by ICAO in Annex16 volume II), experienced within both commercially available and bespoke sampling systems.
2. Impact of cleanliness of Cyclone on uncertainty of nvPM measurements
3. Intercomparison Studies of nvPM mass, number & size instruments using 'novel' particle sources
    - Including fluence measurements of 'novel' surrogate mass calibration sources
4. Understanding Charge potential of aerosols and their impact on particle size measurement
5. Characterisation of particle loss in Splitter 1, given the known issues with maintaining unform flow split velocity across different power conditions

As an outcome of undertaking and interpreting these empirical measurements, a number of findings and recommendations are provided. In terms of understanding potential differences in the temperature gradients in the dilution box (Module 2), it was found that different heating and control strategies and Splitter 1 designs resulted in variations in temperature at Diluter 1 inlet. It was found that some system designs were capable of meeting the 145 °C minimum temperature requirement, however in such cases this was achieved by the control system elevating the temperature between Splitter 1 and Diluter 1 inlet, which is not conducive to minimising thermophoretic loss. As such the definition of T_1, in SAE ARP 6320, was further clarified ensuring it is comparable between different systems towards consistently defining thermophoretic loss for regulatory reporting. However, this work has highlighted that further work is required to better understand the actual particle loss observed from probe inlet to Diluter 1 outlet across different system designs, to enable these losses to be more accurately calculated in future loss correction methodologies.

Operability improvements were noted across both the Swiss and European (EUR) nvPM systems by increasing the frequency of cyclone cleaning, particularly when measuring low mass concentrations. It was observed that 'shedding' from the sharp-cut-point cyclone trap, resulted in increased measured concentrations, in the order of the quoted limit of detection of the mass analysers. Therefore, at concentrations close to the limit of quantification, this resulted in increased uncertainties. It was therefore recommended that advisory guidance regarding cyclone cleaning was added to ARP 6320, to improve the uncertainty in mass reporting at low mass concentrations. In terms of number reporting the cyclone cleaning was not observed to significantly improve cleanliness checks. However, as an outcome of determining this, it was observed that cleanliness issues in Diluter 1 could result in a system not achieving the cleanliness thresholds defined in the standards.

In the absence of a defined gas turbine aerosol standard, capable of acting as a calibration source for all nvPM analysers and enabling empirical validation of sampling and measurement efficiencies of regulatory nvPM systems, several laboratory-scale particle generation sources were investigated across size ranges relevant to gas turbine combustion sources. Sufficiently high particle concentrations were achievable to enable a thorough characterisation of both system loss (including VPR) and number counter performance. However, whilst investigating very small surrogate aerosols (<15nm), at low particle concentrations, significant increases

in uncertainty were observed comparing two nominally identical number counting devices. Use of these novel particle generators allowed comparison of different particle size analysers, highlighting general agreement within a coefficient of variation (i.e., standard deviation/average) of 8.3% for GMD across all test points and 3.4% for GSD within a size ranging from 8 to 75 nm. This result gives confidence that improved system loss correction may be achievable by employing well characterised 'real-time' particle sizers.

It was observed that the charge state of the aerosol can impact fast sizing instruments, which only employ a single unipolar charger, therefore further work is required to understand charge potential of aircraft exhaust. However, it was shown that adding an additional neutralising stage could negate the impact of particle charge.

Nebulised Carbon Black suspensions were successfully demonstrated as a potential 'field check' source for number, mass and size instruments, however further work is required to understand stable concentration limits in solution, charge state and reproducibility of manufacture and repeatability of usage over time[1]. Laser fluence measurements were obtained on numerous particle sources highlighting that nebulised Carbon Black suspensions may be a candidate for future calibrations of Laser Induced Incandescence analysers.

Operating Splitter 1 across a limited range of flow split velocities resulted in only a 3% difference in mass and number concentrations. However, it is noted that further work is required on full engines, investigating a broader range of Splitter 1 geometries and splitter leg velocities, to ensure uncertainties associated with preferential flow and impaction are not currently being under predicted.

[1] Further Discussed in SAMPLE IV Deliverable Report 3.

TABLE OF CONTENTS

LIST OF FIGURES

LIST OF TABLES

LIST OF ABBREVIATIONS

APC	Advanced Particle Counter
BC	Black Carbon
CAPS	Cavity attenuated phase shift
CH	Swiss (nvPM reference system)
CPC	Condensation Particle Counter
DMS	Differential Mobility Spectrometer
eBC	Elemental Black Carbon
EEPS	Engine Exhaust Particle Sizer
EUR	European (nvPM reference system)
GMD	Geometric Mean Diameter
GSD	Geometric Standard Deviation
LII	Laser induced incandescence
MAC	Mass Absorption Cross-section
MSS	Micro soot sensor
NAS	Nebulised Aircraft Soot
NCB	Nebulised Carbon Black (nano-Particles)
NRC	National Research Council Canada
nvPM	Non-volatile Particulate Matter
PSL	Polystyrene Latex (Spheres)
rBC	Refractory Black Carbon
SAG	Spark Ablated Graphite (nano-Particles)
SMPS	Scanning Mobility Particle Sizer
SPG	Silver Particle Generator (silver nano-Particles)
TC	Thermocouple
UDAC	Unipolar Diffusion Aerosol Charger

Table 1: SAMPLEIV Consortium Partners Abbreviations

SAMPLEIV Consortium Partner	Abbreviation
CARDIFF UNIVERSITY	CU
ROLLS-ROYCE PLC	RR
THE UNIVERSITY OF MANCHESTER	UoM
ZURICH UNIVERSITY OF APPLIED SCIENCES	ZHAW

1. Introduction

As of CAEP/10 (February 2016) an inaugural engine nvPM certification requirement and emissions standard for engines of thrust >26.7kN was adopted into the ICAO Annex 16 Volume II as a new Chapter 4 & Appendix 7. The certification requirement specified a standardised sampling and measurement system, as detailed in the schematic provided in Appendix 7 of Annex 16 Vol II and provided below in Figure 1, was developed to enforce a maximum nvPM mass concentration whilst requiring the reporting of LTO nvPM mass and number for in-production engines as of January 2020. Subsequently this same sampling and measurement system was employed as part of CAEP/11, to define new LTO nvPM regulatory limits for both nvPM mass and number, with new type engine applicability required from January 2023.

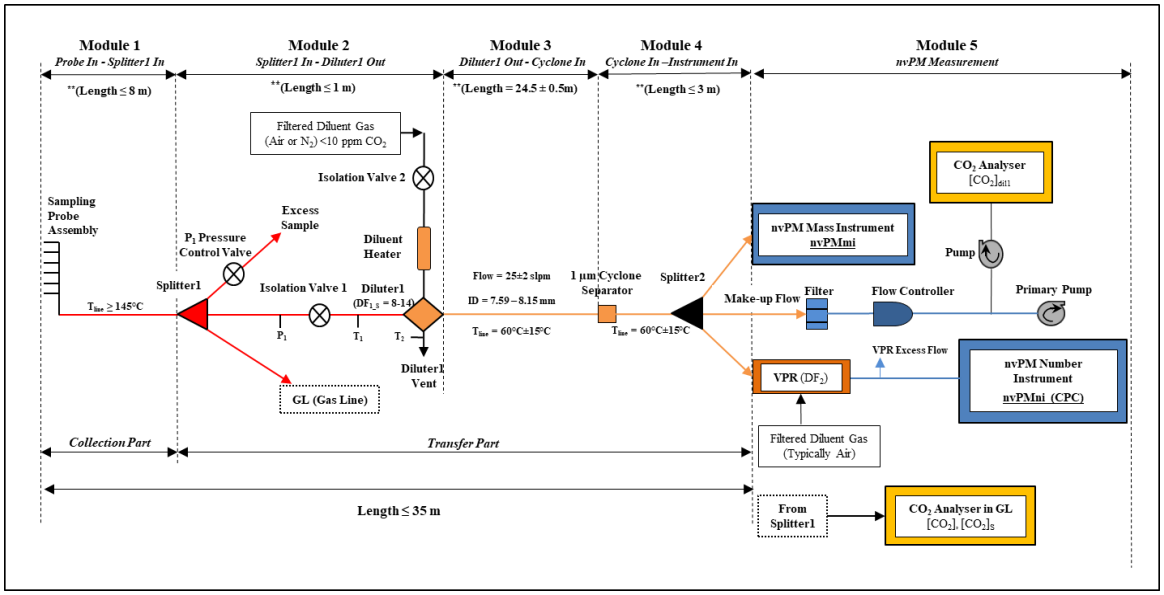

Figure 1: ICAO Annex16 Vol II nvPM Sampling and measurement system

To understand potential improvements that could be made to the ICAO Annex 16 vol. II nvPM sampling and measurement standards and system loss correction reporting (baseline system), a series of experiments were designed and conducted at both Rolls-Royce Derby and Cardiff University's Gas Turbine Research Centre (GTRC) in 2021/22. In consultation with EASA and the relevant SAE E31 teams and sub-committees, several specific independent experiments were proposed to assess:

1. A reported issue of adverse temperature gradients (thermophoretic loss) and compliance in meeting the 145°C minimum temperature at T_1 in the dilution box (Module 2) of nvPM sampling systems
2. Impact of cleanliness of Cyclone on uncertainty of nvPM measurements
3. Intercomparison Studies of nvPM mass, number & size instruments using 'novel' particle sources
    - Including fluence measurements
4. Understanding Charge potential of aerosols and their impact on particle size measurement
5. Characterisation of particle loss in Splitter 1

2. Assessment of T_1 in three 'compliant' nvPM sampling systems

It was reported in SAE E31P discussions, that numerous nvPM sampling systems designed and built to be compliant with ICAO Annex 16 Vol II may not be meeting the current minimum temperature profile defined for T_1 (DP13 SAE E31 Virtual June 2020), -. Currently this definition is given as *"The nvPM Module 2 line wall temperature (T_1), to within 5 cm of the Diluter 1 mixing plane, shall be maintained at greater than or equal to 145°C"*. Given T_1 is not necessarily measured within 5 cm of the mixing plane (as indicated in figure A7-3 of the ICAO Annex 16 Vol II Appendix 7 5th edition) and supported by text in SAE ARP6320A *"In order to minimize thermophoretic losses within Diluter1 and provide an interface between two different active heating sections, Diluter1 nvPM Module 2 line wall temperature (T_1), shall be maintained at greater than or equal to 418 K (145°C). Note that T_1 (used for Collection Part thermophoretic loss calculations) does not have to be located directly at the active heating interface"* then there is naturally a potential issue of compliance should T_1 in any given system drop to 145°C, as there will always be further cooling between T_1 and the dilution mixing plane.

Understanding particle losses in Module 2 is one of the highest priorities of the SAE E31 nvPM system improvement items. It is noted that the maximum uncertainty associated with additional thermophoretic loss in Module 2 is predicted to be 8% (160 → 60 °C), with the uncertainty proportionally reducing with increased "lowest" temperature (e.g., 160 → 90 °C = 5.5% additional thermophoretic loss; 160 → 120 °C = 3% additional thermophoretic loss).

It was also noted that it appeared there was a technical wording error in ARP6320A, defining that T_1 temperature >145 °C is required to minimise thermophoretic losses within the diluter, whereas this temperature is required to minimise thermophoretic loss prior to the diluter – given minimisation of particle loss within the diluter would require a T_1 of 60 °C.

Therefore, experiments were performed in which the temperature profile within Module 2 **Error! Reference s ource not found.**of a regulatory nvPM system (i.e., inlet of dilution box to Diluter 1 inlet as indicated in Figure 1) was characterised by measuring both the gas and inner wall temperature at a range of conditions representative of regulatory aircraft nvPM emission measurement (i.e., inlet temperature ~145-180 °C, flowrates ~20-70 LPM).

The aim of the experiment was to understand the temperature gradients within the EUR and Swiss nvPM reference sampling systems in addition to a commercial system designed and built by Scitek consultants for Rolls-Royce to perform engine emissions certification. By empirically measuring temperature distributions of the three systems, which each had a different heating and insulation strategy, it was possible to assess whether these systems (which were originally designed to meet SAE AIR6241) currently meet compliance and whether the current definition of T_1 is optimal. An understanding of T_1, and the associated temperature profile to this point within Module 2 is required to understand thermophoretic loss, towards reducing the uncertainty associated with system loss correction.

Nominally identical temperature validation experiments were performed on both the EUR and Swiss reference systems at the GTRC prior to combustion testing undertaken December 2021. With the temperature, within the sample flow path of the retrospective Module 2's, measured using two traceably calibrated thermocouples namely:

- A Type K twin bore ceramic thermocouple (TC) 0.5mm diameter wire x 500mm long with 3mm diameter ceramic insulation (TC direct 409-010). This TC was used to measure the gas temperature as its tip remained in the centre of the pipe thanks to the ceramic coating.
- A Type K 310 Stainless Steel Sheath Thermocouple (SS TC) 1.0mm diameter x 750mm long (TC direct 408-060). This TC was assumed to be measuring the inner-wall temperature (or gas temp. close to wall) given it was in contact with the inner surface.

Replicating real-world conditions (positive pressure at inlet of Dilution Box), elevated temperatures (>160 °C) was achieved using compressed air and a Watlow CAST-X 500 air preheater which was plumbed to the front of each reference system dilution box during their respective testing. The inlet air temperature was regulated using a fixed TC located in the gas stream between the air heater and inlet of the dilution box. Variable flow rates at Splitter 1 were facilitated using a mass flow meter attached to the outlet of the systems respective spill lines, which measured the flowrate going through the spill line when opened (simulating flow conditions witnessed on engine tests at higher thrust conditions).

A temperature reader (TC direct 305P) which firstly afforded in-house calibration, was used to read both the TC's (wall and gas stream) sequentially. This methodology was adopted as using both TC's in parallel would have caused a large restriction in the sampling line. The temperature reader & TC combinations were pre-calibrated using a traceable dry block (see calibration certificate in Appendix) at 60 °C. Temperature checks were then performed at block set temperatures from 60-180 °C, with the results provided in Table 2. A temperature measurement repeatability experiment was also performed by taking eight successive temperature readings (4 with the ceramic TC and 4 with the SS TC) while the calibrated temperature block was at 60 °C. The readings indicated a measurement repeatability of ±0.2°C (at 60 °C) hence it was determined post experiment correction of measured data was not required (relative uncertainty across temperature <1%).

Table 2: Calibrated values of the Ceramic and Stainless-steel (SS) TCs with the temperature reader

Calibrated Dry block set temperature (°C)	Reader + ceramic TC (°C)	Reader + SS TC (°C)
60	60	60.1
90	90.6	90.5
120	120.9	120.9
150	151.3	151.2
180	180.4	180.4

2.1. EUR Reference system T_1 experiment

2.1.1. Experimental setup

The EUR dilution box has numerous permanent thermocouple locations affording control and recording of the different temperature zones. Figure 2 provides a photograph of the sampling lines (with heaters/ ovens removed) to show the location of the fixed thermocouples (green markers) used on the nvPM sample line and diluent control system along with a schematic to indicate the location of a temporary 'internal' thermocouple used to assess the temperature gradient within the nvPM sample line at four locations (red markers).

As can be seen T_1 in the EUR dilution box is measured between Splitter 1 and the isolation valve (see yellow and green marker in Figure 2) with the thermocouple tip positioned at the edge of the gas stream affording a measure of the gas temperature next to the inner wall, which was nominally the same position as the 'temporary' internal thermocouple when placed at position 2.

The dilution box was set as per normal operation, with the Gas Transfer Line (GTL) heated at 160 °C and sampling 14 sLPM, and the diluter and diluent heated to maintain a diluter vent outlet temperature of 60 °C. Two heating strategies were tested in the EUR dilution box to maintain the temperature from the diluter box inlet and Diluter 1 inlet. The first utilised trace-heating elements controlled at 160 °C directly mounted onto the pipework which were then lagged with insulation and the second employed a 'bespoke' oven-heating setup, with the temperature controlled by maintaining heater pads at the top and bottom of the oven at 180 °C, which it was empirically determined resulted in an internal oven air temperature of 162-165 °C.

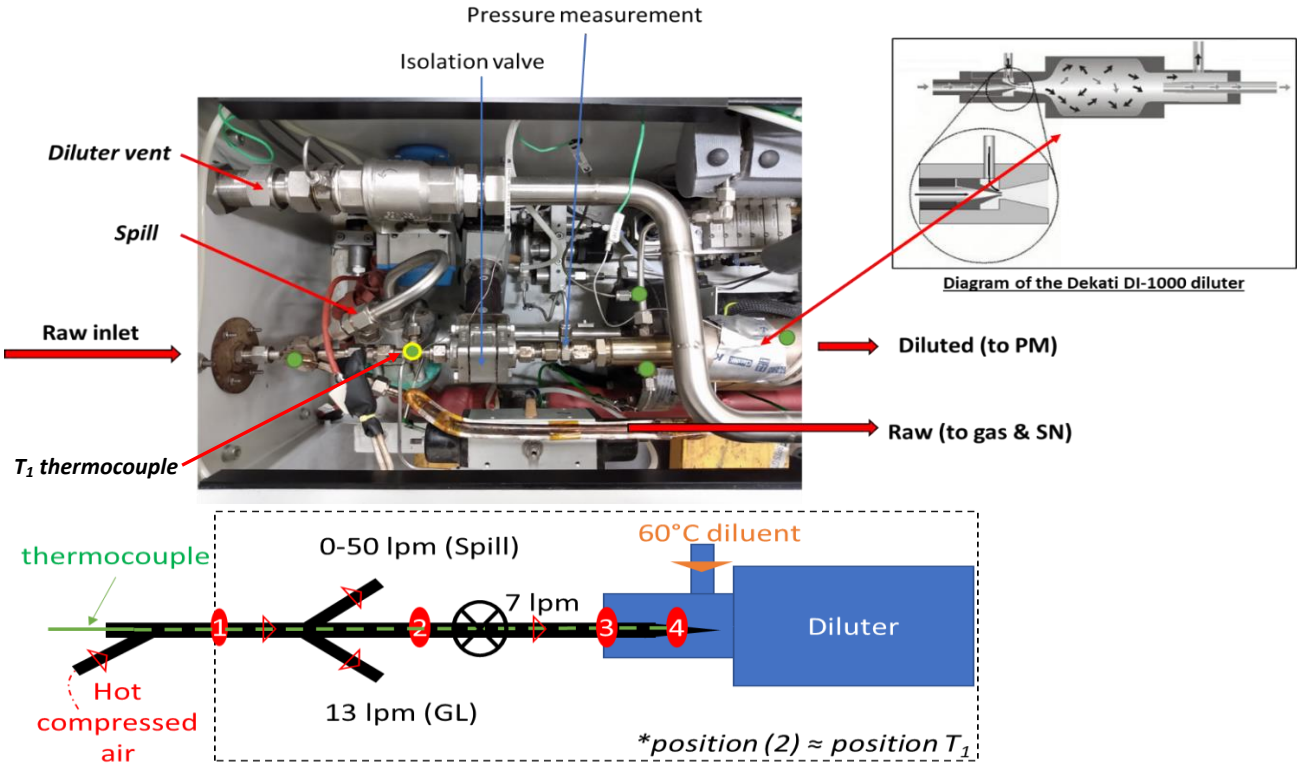

Figure 2: Photograph of the inside of the EUR dilution box, highlighting location of permanent thermocouples (green markers) T1 location (green marker yellow outline) and a schematic highlighting the temporary 'internal' thermocouple locations used in assessing temperature distribution at four positions (red markers)

As discussed previously, regulatory nvPM emission testing conditions were replicated using pre-heated compressed air, affording a range of different inlet temperatures and pressures, with corresponding changes in overall flowrate offered by opening and closing of the pressure spill valve. The spill flow rate was further controlled by increasing the inlet pressure and was recorded using a Coriolis flowmeter.

For the temperature gradient experimentation, measurements were performed by moving the 'temporary' internal thermocouple to four locations within the nvPM transfer line, namely:

- Position (1): inlet of the dilution box
- Position (2): EUR system T_1 position (between Splitter 1 and isolation valve)
- Position (3): Between isolation valve and Diluter 1 inlet
- Position (4): 2cm before diluter nozzle

2.1.2. EUR T_1 Results: Trace-heating Vs. Oven-heating

The temperature profile of Module 2 of the EUR system dilution box was experimentally characterised using the stainless-steel sheath thermocouple (SS TC) (inner-wall temperature) for two heating systems, namely trace-heated or heated oven. The trace-heating experiment was performed prior to the EUR reference systems oven upgrade (Sept 2020) with the thermocouple/temperature reader not traceably calibrated immediately prior to the experiment. The oven-heating experiment was performed in December 2021. It is noted that the oven upgrade was not specifically undertaken to improve the temperature distribution of Module 2 but implemented to facilitate easier access to the diluter for cleaning, with the hope that the temperature within Module 2 would be more homogenous.

It is noted that T_1 as normally reported by the EUR reference system (fixed thermocouple mounted in Swagelok fitting to measure the inner wall gas temperature near position 2 (Figure 2)) fluctuated between 161-164 °C for the trace-heating experiment, and between 155-160 °C for the oven-heating experiment.

Temperature measurements were performed for both the trace-heated (blue) and oven-heated systems (orange) with respective data compared at different temperature and flow settings using the SS TC, presented in Figure 3.

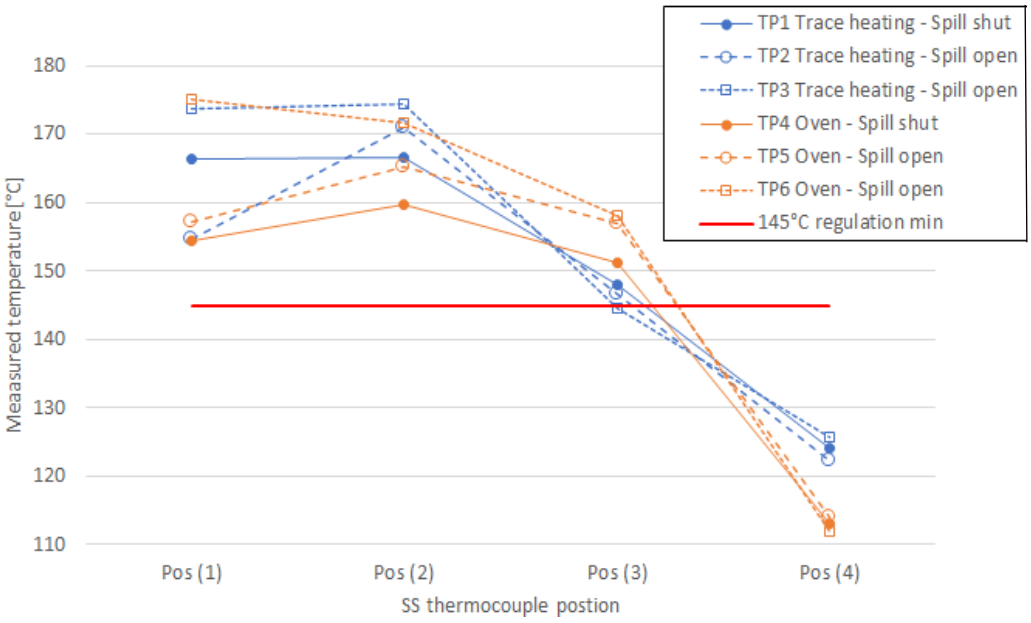

Figure 3: Inner-wall temperature profile in Module 2 of the EUR dilution box (blue: trace-heating; orange: oven heating)

As can be seen, both heating systems are seen to perform similarly, with the temperature being consistently > 145 °C to approximately position (3). However, the temperature gradient through Module 2 was observed to be smaller with the oven-heating system (ΔT< 17 °C) than with the trace-heating system (ΔT< 30 °C), likely owing to the more homogenous heating to diluter inlet offered by the regulated oven space. Note that differences observed between trace-heating and oven heating for position (3) may also be due to slight differences in experimental set-up and temperature reading accuracy between the two tests.

In the case where the inlet gas temperature is lower than the oven set-point of 160 °C (i.e., TP2, TP4 & TP5 in Figure 3) then it is expected that the temperature of the sample gas increases, before again cooling, which from the point of view of additional thermophoretic loss is not ideal. For a scientifically optimum design, towards minimal thermophoretic loss, if the exhaust gas temperature drops to the minimum permissible temperature of 145 °C, then it should not be reheated. However, given the cold junction caused by the coupling of the stainless-steel inlet pipework to the relatively cooler diluter body (60 °C), then achieving 145 °C at T_1 (as currently defined) would not be practically possible, given that there will always be a temperature gradient between Splitter 1 and the point of the dilution.

As can be seen in Figure 3, there is always a significant thermal gradient from position 2 to 4, with lower temperatures at position 4 observed in the case of the oven heating. It is noted that opening the spill valve when the inlet temperature (i.e., position 1) is < 160 °C (i.e., TP2 and TP5), increases the sample flowrate through Module 2, and leads to an increased temperature in position 2 due to increased heat transfer from the pipework to the gas.

2.1.3. EUR T1 Results: Oven-heating gaseous vs inner-wall temperatures

The temperature measurements performed with both the SS TC (inner-wall gas temperature) and Ceramic TC (flow-path gas temperature) are compared for the oven-heated EUR dilution box in Figure 4. The temperature profile is seen to be consistent between the two thermocouples, with the gas temperature recording slightly less fluctuation than the inner-wall temperature (ΔT< 15 °C Vs ΔT< 17 °C). Also, the gas flow temperature at position (4) is seen to be significantly greater than the inner-wall temperature (130-140 °C Vs 110-115 °C). This observation is expected given that the inlet nozzle of the diluter is located in a plenum supplied and surrounded by 60 °C air.

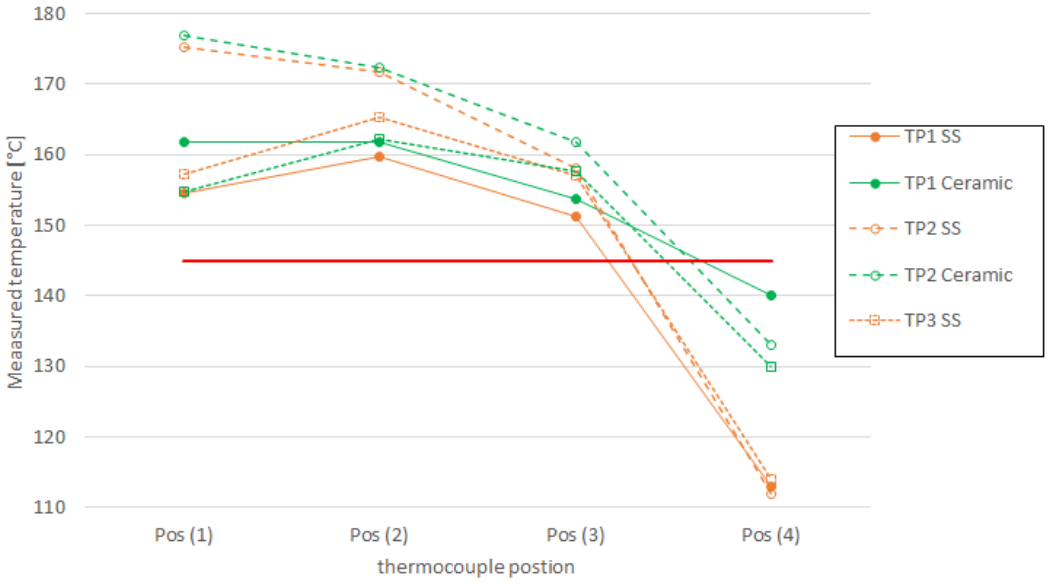

Figure 4: Inner-wall (orange) and gas (green) temperature profile in Module 2 of the oven heated EUR dilution box

As can be seen in Figure 3 and Figure 4 it seems that in the case of both the trace heating and oven heating strategies, compliance to the current definition of T_1 is met. However, as indicated earlier, in the case of low inlet gas temperatures with the spill open, the way this compliance was met is by the control system heating the gas by circa 15 °C before it again cools entering Diluter 1 at position 3. As such in terms of thermophoretic loss this would be equivalent to allowing the T_1 temperature to drop below the 145 °C threshold.

2.2. Swiss Reference system T_1 experiment

2.2.1. Experimental Setup

The diluter box in the Swiss system has two heating zones. As shown in Figure 5, the inlet section of the diluter box, including Splitter 1 and the PM isolation valve, is heated using a custom-made heating jacket (Horst GmbH, Germany). The heating jacket and the temperature controller for the Dekati DI-1000 diluter are standard accessory components from Dekati. The thermocouples used to set and control the heaters are located inside the heating jackets. T_1 is measured on the outer surface of Splitter 1 (T1a). In addition, a second thermocouple was installed prior to the experiment on the surface of the short tube section between the PM isolation valve and the Diluter inlet (T1b).

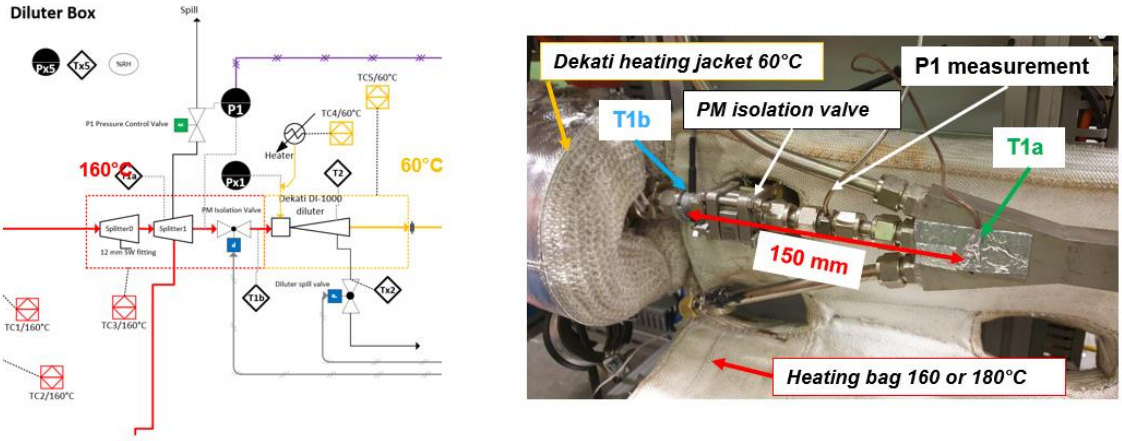

Figure 5: Schematic of the diluter box in the Swiss reference system and location of T1 measurement

As discussed previously, the equipment used for the Swiss system T_1 measurement was identical to the equipment used for the EUR reference system. Figure 6 shows the air preheater setup attached to the diluter box inlet. The P_1 pressure control valve was either closed (with P_1 maintained near ambient pressure) or opened with the compressed air pressure set to achieve spill flow rate of 50 LPM. The flow rate was monitored using a Coriolis flow meter.

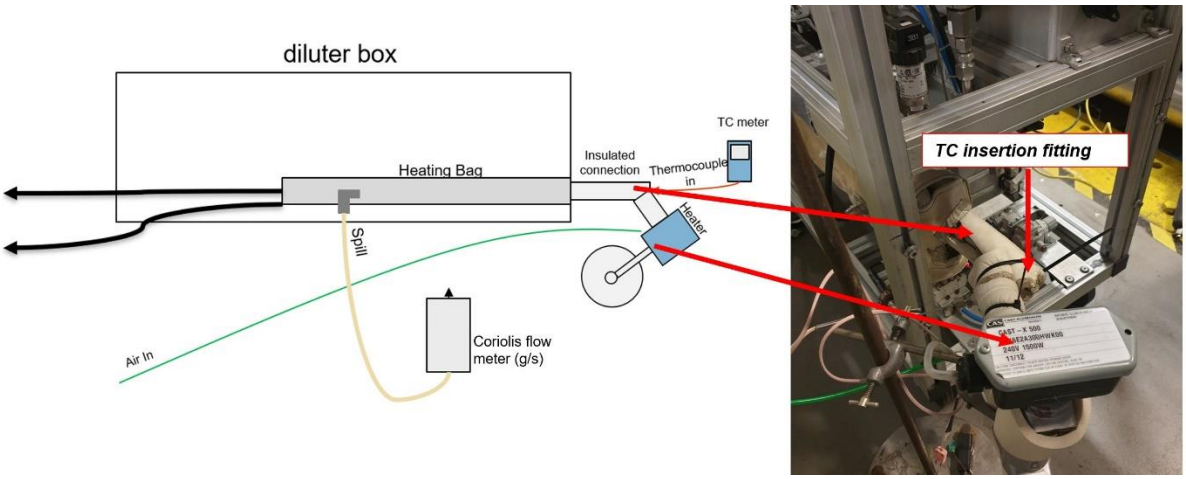

Figure 6: Experimental setup for the T_1 temperature measurement in the Swiss reference system.

The two TCs used during the experiment were inserted up to seven different positions (Figure 7). The ceramic TC could only reach the first two positions: diluter box inlet at 0 cm, and 26 cm with the TC fully inserted. The SS TC was used to measure inner surface temperature at all seven positions. Note that TC insertion point in the air preheater assembly was ~17 cm upstream of the diluter box inlet.

The air preheater was set to temperatures between 140 °C (cold) and 180 °C (hot). The heating jacket for the diluter was kept at a constant setpoint, whereas the heating jacket in the inlet section was set to 160 °C or 180 °C. The measurements were taken after stabilisation of the preheater and heating jacket temperatures. At each test point (varying spill flow, preheat temperature and heating jacket temperature) each TC position was measured twice. The TC was inserted stepwise to each position and the same position was measured during retraction.

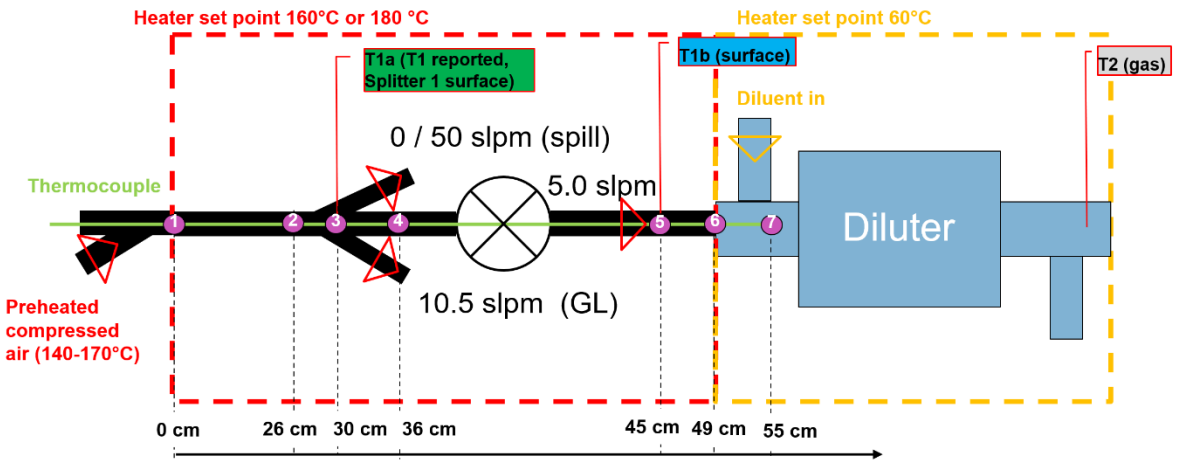

Figure 7: Schematic of the diluter box and T1 measurement positions

2.2.2. Swiss System T_1 Results

The results of the T_1 measurement using the two thermocouples are shown in Figure 8. The squares show the results obtained with the SS TC and the circles are the results obtained with the ceramic TC. For all test points, the temperatures at positions 1 and 2 with the two thermocouples were within 5 °C. The black and red symbols represent measurements with the heating jacket set to 160 and 180 °C, respectively. The green and blue rectangles at positions T1a (note that this is the T_1 reported by the system) and T1b are the ranges of temperatures measured during the experiment.

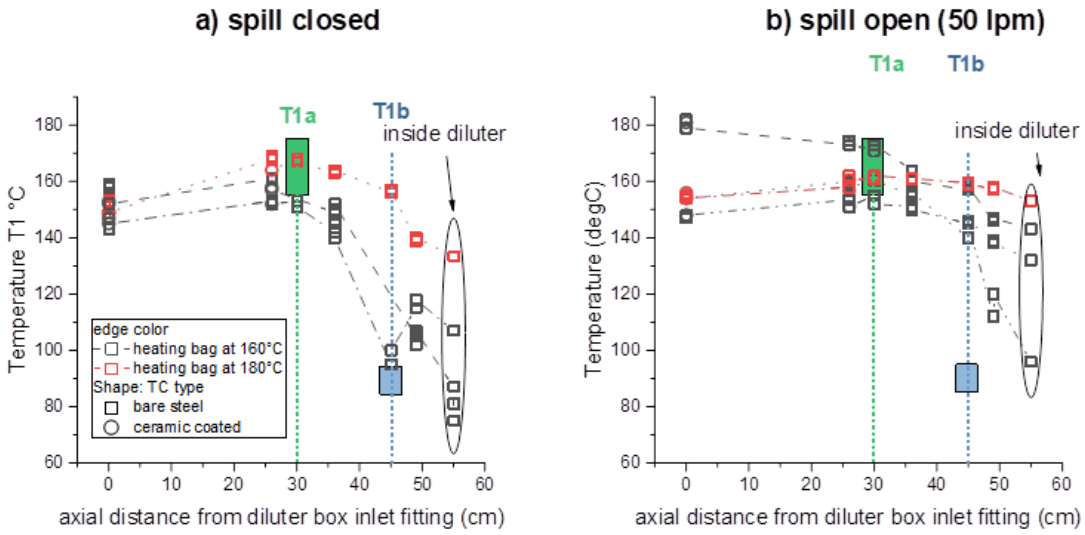

Figure 8: Results of the T1 measurement in the Swiss reference system.

Considering the case with the spill closed (Figure 8a), the preheater was sequentially set at two temperatures namely, its nominal setting (~160 °C) and cold set-point (~145°C). In both cases, the temperature between positions 1 and 3 increased, similar to the findings from the EUR system shown above. The ΔT between 1 and 3 was up to 15 °C larger with the heating jacket set to 180 °C. Downstream of the PM isolation valve (position 5), the temperature decreased steeply. The PM isolation valve acts as a heat sink and due to its insufficient heating (heated only from one side by the heating jacket). Interestingly, the temperatures downstream of the PM isolation valve were up to 60 °C higher, with the heating jacket set to 180 °C. The reason for this significant difference with a relatively small change in heater setpoint is unclear.

With the spill open and the air preheater set to nominally cold (145 °C) and hot temperatures (180 °C), similar trends were observed upstream of the PM isolation valve as witnessed with the spill closed (Figure 8b). The

ΔT between positions 1 and 3 were lower than with the spill closed by circa 5 °C. As seen with the air preheater set to nominally hot (180 °C), a ΔT of -10 °C was observed between positions 1 and 3. In contrast to the measurements with the spill shut, the temperatures at positions 4 to 7 were significantly higher. This can be explained by the high flow rate of hot air actively heating the Splitter 1 assembly and subsequent conduction to the PM isolation valve, resulting in the sample at Diluter 1 maintaining a higher temperature. Also, with the spill open, the differences between the measurements with the heating jacket at 180 °C and 160 °C were smaller than witnessed with the spill closed.

These findings suggest that keeping the heating jacket at 180 °C prevents a significant drop in exhaust sample temperature between the PM isolation valve and the diluter inlet. For the outer tube surface temperatures, only the T1a (T_1 in the Swiss system) was above the minimum required 145°C at all test points. T1b was in the range from 80 to 100 °C, however this is noted to be an outer wall pipe temperature and as observed, particularly in the case of spill open, was significantly lower than the comparative in-gas temperature measurements which are more representative for thermophoretic loss correction. The same conclusions could be drawn based on the subsequent tests with the complete nvPM reference system on the RQL rig (Figure 9, heating jacket at 180 °C). The spikes and drops in T1b correspond to periods with the PM isolation valve closed (cleanliness check, fuel change).

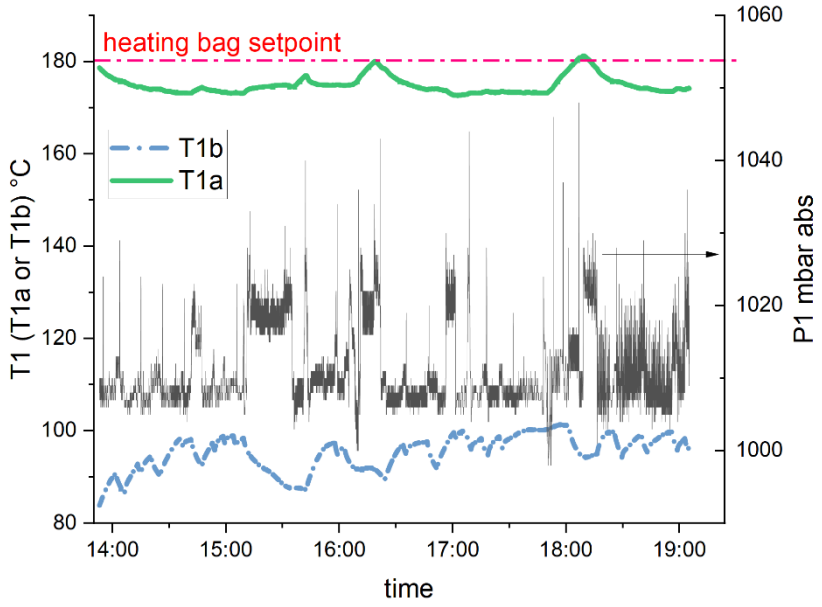

Figure 9: T1a and T1b (left) and P_1 (right) as a function of time during nvPM testing using the RQL rig

2.3. Rolls-Royce nvPM system T_1 experiment

2.3.1. Experimental Setup

Rolls-Royce assessed their Scitek nvPM system dilution box temperature distributions by adding 10 surface-mounted NIST traceable thermocouples in addition to designing a bespoke NIST traceable in-gas temperature sensor which was placed in the gas stream immediately prior to the diluter inlet as shown in Figure 10. This TC was potted in an insulating medium to ensure conduction effects from the sealing assembly were minimised and sized appropriately to meet 10:1 immersion length to TC diameter ratio (Industry best practice). As can be seen in normal configuration T_1 is typically controlled and logged at the inlet to Splitter 1 at a location 370 mm upstream of the dilution mixing plane.

To replicate representative test inlet gas conditions, compressed air was supplied to a thermostatically controlled 25 m heated line providing a diluter box inlet gas temperature of either 145 °C or 175 °C (minimum and a hotter inlet). The Gas Transfer line was set at 12.7 sLPM and the spill closed to provide a worst-case

temperature loss scenario. Initially the system was set to standby with heaters activated with the isolation valves close, before the system was put to 'run' mode whereby the isolation valves opened, and gas flows were initiated. Real-time data was logged across the whole test sequence to assess the times taken to reach thermal equilibrium.

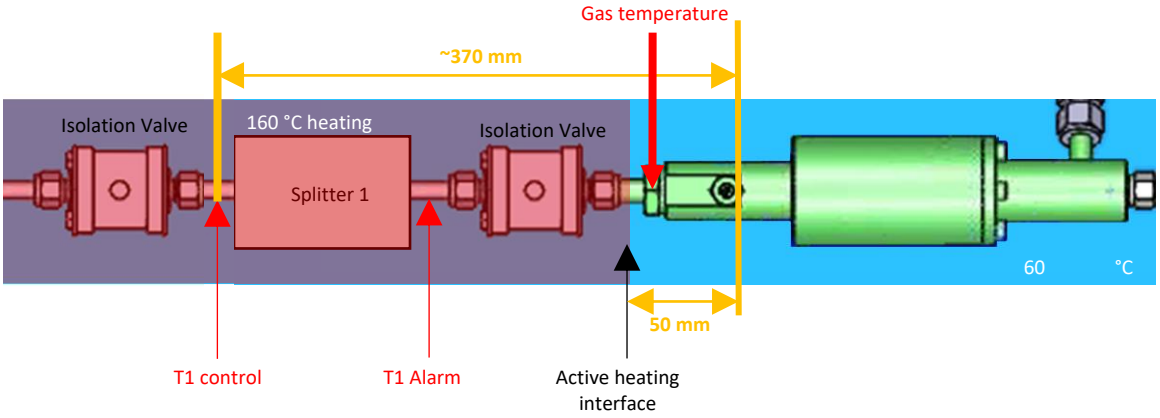

Figure 10: Schematic Representation of Rolls Royce Diluter box highlighting locations of the standard T_1 measurement and additional in-gas measurement site

2.3.2. Rolls-Royce T_1 Results

As discussed previously and seen in Figure 11, the experiment was started initially with the system in standby, whereby the active trace heating was energised with the gas flows off and left to stabilise. At approximately 10:30 the first isolation valve was opened allowing flow to enter the Gas Transfer Line (GTL) leading to a sudden increase in the dilution box inlet temperature (brown dashed line) as air heated by the 25m line entered the dilution box. As can be seen initially this was set at 145°C which was considered worst case in terms of meeting the T_1 compliance.

At approximately 10:55 the system was put into 'run' mode meaning all isolation valves opened and flow though the nvPM system was initiated. As can be seen at this time, large variations in the diluent heater temperature are observed (dark blue line), thought to be because of the legacy Annex 16. Vol II compliance with regard to requiring temperature control using T_2, whereby the slow response time between the heater increasing temperature and the diluter outlet temperature rising leads to significant overshoot of the heater body temperature. In the latest CAEP agreed revision of Annex 16 Vol II (5th edition July 2023) this requirement has been removed; hence this temperature control strategy is currently being assessed by Rolls-Royce.

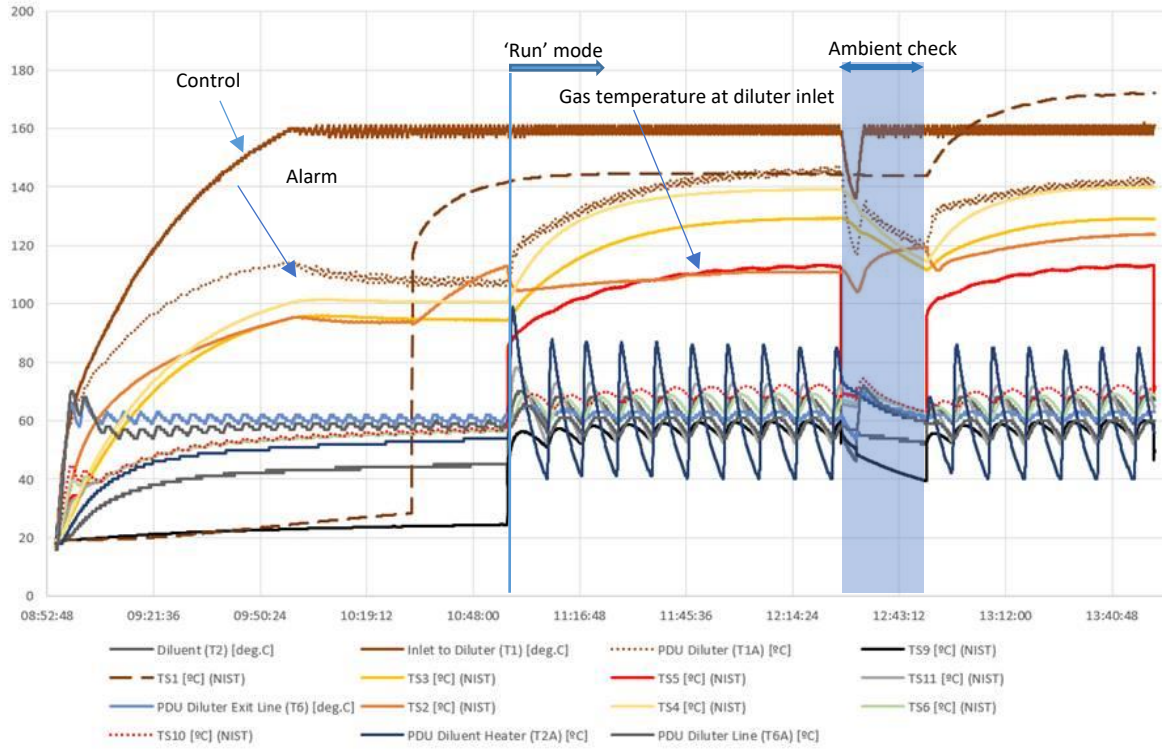

Figure 11: Temperature measurements in Scitek nvPM Dilution Box

It is observed that at constant condition it takes approximately an hour for the gas temperature at the diluter inlet to reach a pseudo constant temperature of 115 °C, whilst noted that this is considerably lower than the 160 °C and 145 °C witnessed at the T_1 control and alarm locations. Also, the time taken for Splitter 1 (yellow lines) and T_1 control to rise suggest that Splitter 1 has significant conduction losses via the spill lines when flow to the spill leg is isolated. Similarly, given the fact that the T_1 control temperature is higher than the splitter temperatures indicates that the second isolation valve is warmer than the splitter, suggesting either it has a higher heating rate and/or lower conduction losses. At 12:30 a standard ambient check is performed, whereby the isolation valves both shut causing the flow in both the nvPM and GTL to cease leading to the witnessed reductions in temperatures.

At 12:50 the system is again switched to 'run' mode with the gas inlet line increased to the 'hotter' 175 °C temperature. As seen, this has the unexpected effect of actually resulting in lower Splitter 1, T_1 alarm and diluter inlet gas temperatures. This result highlights that the control T_1 is now largely kept warm by the inlet gas, resulting in the trace heating not being energised leading to witnessed drops in temperature at the splitter and second isolation valve, brought about by the aforementioned conduction losses from Splitter 1 to the spill line.

As such it is observed that with the spill closed the Scitek nvPM certification system used by Rolls-Royce is not achieving the 145°C threshold at Diluter1 inlet. However, the data highlights that there are significant thermal losses occurring at Splitter 1 as a result of the sophisticated multi-leg spill system. It is therefore perceived that in the case of an engine test with expected inlet gas temperatures at or above 160 °C and sufficient (much higher) flows through the spill system, that the splitter, and hence subsequent downstream isolation valve, would heat to higher temperatures than were experienced in this worst-case (zero spill flow) laboratory test.

Table 3: Description of temperature measurement locations in Figure 11

	Thermocouple Ident	Location	Thermocouple position
Permanent system temperature measurements/ alarm monitors during Engine Testing	T1	Splitter 1 inlet	Surface mounted
	T1A	Between Splitter 1 and Diluter isolation valve	Surface mounted
	T2	Diluter vent	In Gas
	T2A	Diluent heater	In Gas
	T6	Diluter sample outlet	Surface mounted
	T6A	Diluter box sample outlet	Surface mounted
Temporary temperature sensors added for laboratory study	TS1	Dilution box inlet temperature	Surface mounted
	TS2	Splitter Spill	Surface mounted
	TS3	Splitter 1 inlet (outer wall)	Surface mounted
	TS4	Splitter 1 outlet (outer wall)	Surface mounted
	TS5	Diluter inlet fitting	In gas – thermally isolated
	TS6	Diluter body - inlet	Surface mounted
	TS7	Diluter body - front	Surface mounted
	TS8	Diluter body – end	Surface mounted
	TS9	Diluter outlet fitting	Surface mounted
	TS10	Diluter inlet fitting	Surface mounted
	TS11	Diluter Gas Inlet	In gas

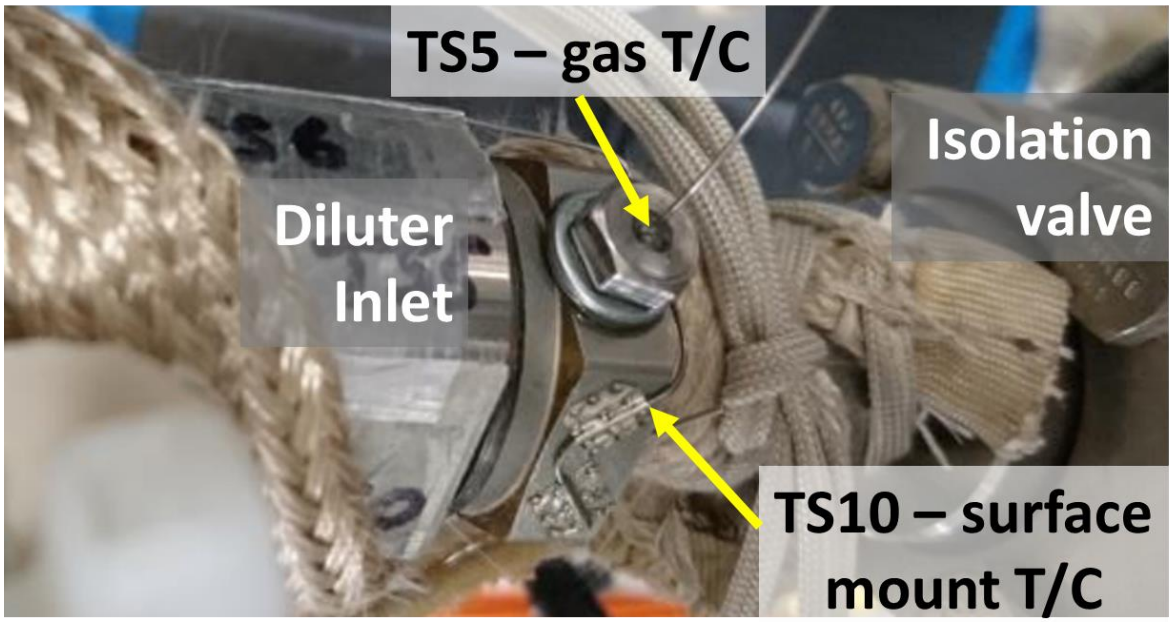

Figure 12: Photo of Diluter inlet showing bespoke drilled-through, thermally isolated thermocouple for sample gas temperature measurement & wall surface mounted temperature measurement (prior to install of insulation)

The upstream conduction effect of the diluter body can be observed by the TS5 (solid red – Figure 11) and TS10 (dotted red – Figure 11) temperature measurements at the same location right at the interface between the two active heating zones (TS5 in the gas and TS10 on the fitting wall as shown in Figure 12). The significant difference between them (~80 to 85 °C) shows the impracticality of using wall surface mounted TC's close to the diluter to determine the 'real' thermophoretic particle loss in the gas sample.

2.4. Conclusions of T_1 Assessment

Lessons learnt from these three experiments were reported to SAE E31. Supported by the work of Missouri University of Science & Technology, who also performed a similar experiment on the North American Reference System (DP34 SAE 31 On-line January 2021) this work formed a significant part of the evidence which led to an interim change in specified T_1 location in SAE ARP6320B and then into ICAO Annex 16 Vol II[2]. This interim solution standardises the thermophoretic loss correction used by all engine manufacturers in regulatory nvPM Emission Indices reporting (Probe to Splitter1) whilst ensuring consistency for existing data in the ICAO Aircraft Engine Emissions Databank.

However, due to additional thermophoretic particle loss witnessed between Splitter1 and Diluter1 inlet (given the known temperature gradient) and the expectation of additional particle loss within Diluter1, these particle losses have subsequently been added as part of the recommended practice for calculation of system loss correction factors during the revision of SAE ARP6481A.

It is noted that this is an interim solution until further work is performed, this calculation consists of a simple thermophoretic calculation between Splitter1 (T_1) and the specified 333 K (60 °C) Diluter1 outlet temperature. Depending on a specific nvPM system design this interim solution may be slightly overestimating or underestimating particle loss in Module 2.

To reach a scientifically robust particle loss correction for Module 2 requires understanding of system temperatures between Splitter1 and Diluter1 inlet. Some nvPM systems have temperature measurements in this section which may help. However, as discussed pipe temperatures do not accurately quantify sample gas temperature, therefore it is likely that detailed experiments following the methodology for the EUR and Swiss nvPM systems may need to be performed on individual nvPM system designs to quantify the experienced

[2] Discussed further in Section 1.4.3 - SAMPLE IV Deliverable Report 2

thermophoretic loss. In addition, further validation of Diluter1 loss (empirical measurements supported by CFD) is required.

Also, as a result of this work, additional wording concerning 'negative temperature gradients' was added to both SAE ARP6320B and ICAO Doc 9501, towards minimising the chance of additional unintentional thermophoretic loss.

3. Impact of cleanliness of cyclone on nvPM measurements

As part of the SAMPLE I (2009)[3] findings, a 1 µm cyclone was specified as required for the nvPM sampling system to ensure that large 'shedded' particles were not included in the mass averages, given a few large particles were seen to significantly impact average concentrations on a steady condition in the case of an LII-200 instrument. Similarly, it was thought that additional protection of the flow orifice contained within CPCs was warranted. However, during full-scale engine testing it has recently been observed that shedding of particles from the cyclone collection pot, has led to failed cleanliness checks during nvPM tests (cleanliness maximum limits are 1 µg/m^3 and 2 particles/cm^3). It has been suggested this problem is most pronounced on a low concentration test point following a test condition with a higher nvPM mass loading.

During RQL combustor rig testing, which it is noted experiences high incidences of large particle shedding from within the combustor (engine testing may or may not have same high shedding frequency), frequent cleanliness checks were performed towards understanding the impact that cyclone cleanliness may play on nvPM measurement uncertainty particularly at low mass concentrations. After failed cleanliness checks, the cyclone collection pots were removed, and cleaned out with isopropanol and cleaning tissue before replacement.

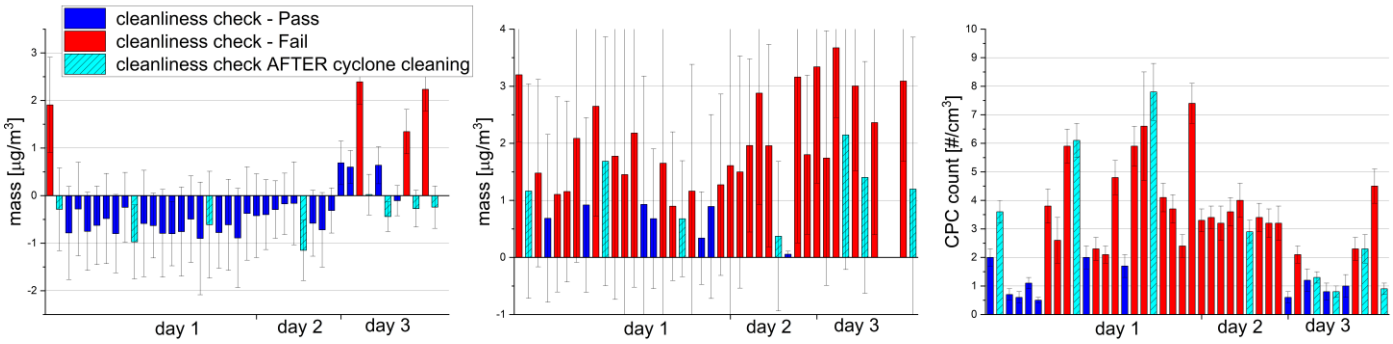

Figure 13: EUR nvPM reference system cleanliness checks performed in between test points before and after cleaning the 1µm cyclone over three days of rig testing (MSS left, LII-300 centre, APC right)

Figure 13 shows the multiple cleanliness checks performed by the EUR system for the MSS, LII-300 and APC performed in between test points at regular intervals over the course of three days of combustor rig testing. As can be seen, cleaning the cyclone collection pot always reduces the reported LII-300 and MSS mass with lower mass observed after cleaning. However, cleaning the cyclone doesn't appear to have an impact on the APC cleanliness checks, as would be expected given it is thought the cyclone sheds only a few large particles ~ 300 nm when dirty. It is also seen in Figure 13 that the MSS generally reports a value < 0 µg/m^3 during cleanliness checks; It is suspected this is due to the MSS resonance check being performed on the sampled exhaust to provide accurate mass reading, with a differing gas composition experienced during cleanliness checks due to it being composed of diluent gas and therefore correcting for different interference. This highlights that the MSS should be resonance checked on the diluent prior to a cleanliness check and then back on the combustion source when measuring exhaust. However, it is noted that resonance checks typically take around 2 minutes to perform, which may mean it is not practical to do regularly, particularly at high engine powers during engine certification testing. Cleanliness checks were performed regularly throughout the test

[3] Petzold et al. (2009) SAMPLE I Final Report - https://www.easa.europa.eu/en/document-library/research-reports/easa2008op13

days, at a much higher frequency than required in ICAO Annex 16 Vol II which is annually. It is noted that during these numerous checks the LII-300 and APC failed the certification cleanliness check threshold, which is thought to result from a contaminated diluter, which was subsequently cleaned after the test campaign with cleanliness check concentrations returning to expected values.

Cleanliness checks for the MSS and APC in the Swiss system can be seen in Figure 14. It can again be observed that the cyclone collection pot cleaning improved the reported cleanliness. It is noted that although the cyclones in both systems are nominally identical (BGI SCC), they are mounted in different orientations with the Swiss mounted vertically and the EUR mounted horizontally, which is thought to have negligible impact as the centrifugal forces are assumed to be dominant compared to gravitational forces. On day 2, the MSS reported negative values during cleanliness checks, which again may be linked to the resonance check being performed on the diluted exhaust sample instead of pure diluent, as described above for the MSS in the EUR system. In comparison to the EUR system, the APC cleanliness failed only during the first cleanliness check on day 1 and the cyclone collection pot cleaning improved both mass and number cleanliness.

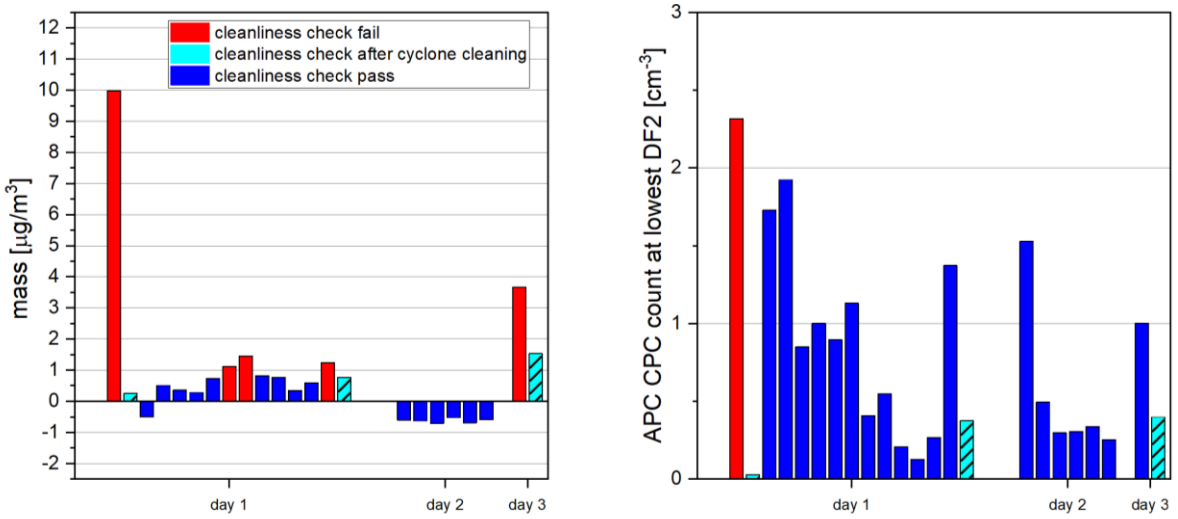

Figure 14: Cleanliness checks of the Swiss nvPM reference system (a) MSS (b) APC performed on 7, 8 and 9 December 2021

To determine the size of the particles contributing to the increases in concentrations from the 'dirty' cyclone, a Fidas Frog optical scattering particle sizer was added to the Swiss sampling system operating in parallel with the nvPM instruments. The instrument reports PM1, PM2.5 PM4 and PM10 concentrations as well as size distributions in the optical size range from 180-930 nm. The mass concentrations measured during a cleanliness check before and after cyclone cleaning are shown in Figure 15.

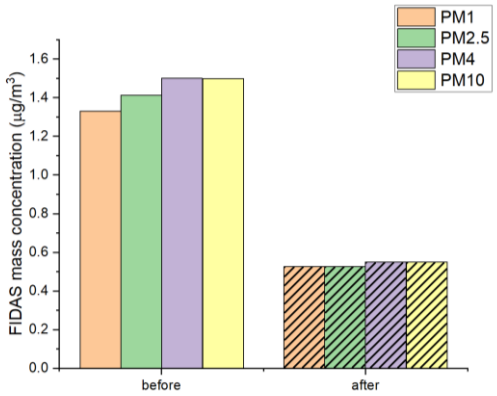

Figure 15: Mass concentration reported by the portable optical sizer FIDAS Frog during cleanliness checks before and after cyclone cleaning

It can be seen in Figure 15 that the vast majority of the particles shed from the cyclone, either before or after cleaning, are captured within the PM1 size classification, with a negligible contribution of particles larger than 2.5µm (note that the measurement uncertainty of this instrument has not been evaluated). As such this highlights that the use of an optical scattering sizer can be a useful diagnostic tool to assess system cleanliness.

From this work it was recommended that advisory guidance regarding cyclone cleaning was added to SAE ARP 6320 and ICAO Annex 16 Vol II,

4. Particle Sources

A number of aerosol sources were appraised for nvPM measurement in-field checks and calibration to improve uncertainty including consistency. Particle sources included a recently released commercially available VSP-G1 nanoparticle generator[4], a commercial Catalytic Instruments Silver Particle Generator (SPG)[5], nebulised COTS traceable standards (gold, silica) and Carbon Black powders (manufactured and aircraft engine sources); and a bespoke non-proprietary combustor rig designed and operated by Cardiff University at its Gas Turbine Research Centre (GTRC). Brief details of the sources are described below.

4.1. VSParticle generator

The VSParticle, shown in Figure 16, is a commercially available user-friendly, tabletop nanoparticle generator based on spark ablation technology. A loaned instrument, with both gold and graphite electrodes, was kindly made available, by the instrument OEM, to the SAMPLE IV consortium to trial as a useful particle source towards calibration and intercomparison of nvPM mass, number, and sizing instruments.

Figure 16: Photograph of VSParticle nanoparticle aerosol generator

This particle generator offers a wide versatility of available particle materials, which it is claimed is key for reducing research iteration times and provides flexibility. The VSParticle allows efficient changes of aerosol material via changing of the instrument's electrodes. This methodology is stated to allow the creation of repeatable and stable aerosols of pure or bi-metals/alloys, along with other conductive materials such as Graphite in an aerodynamic size range of 1 to 300nm, without the requirement for surfactants or risk of residual peaks of contaminants (often found in nebulised particle solutions). The VSParticle is similar in technology to the PALAS spark particle generator but has finer control over the particle generation.

Prior to use in SAMPLEIV, the company provided a demonstration of the generator for both gold and graphite particles with preliminary data being collected using a Cambustion DMS500 to interrogate the size ranges and number concentrations achievable. Details of the witnessed aerosols sampled after a 10:1 additional dilution stage are presented in Figure 17 with a summary of the instrument set-points required to achieve these distributions presented in Table 4.

[4] https://vsparticle.com/products/vsp-g1-nanoparticle-generator
[5] https://catalytic-instruments.com/wp-content/uploads/2020/09/IRWIN-12.IM_.18.pdf

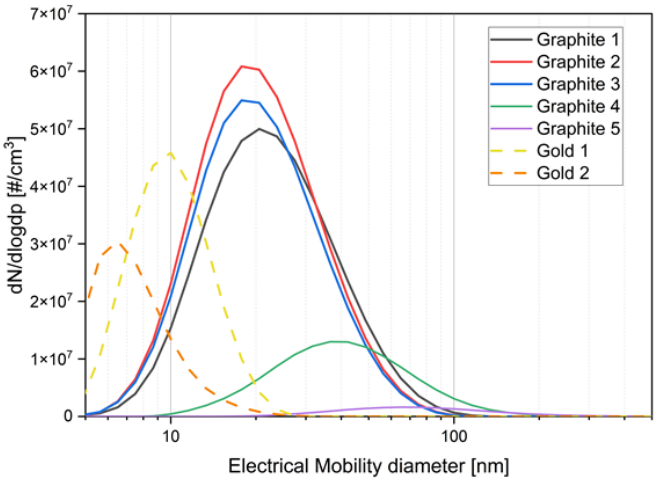

Figure 17: Spark Ablated Graphite (SAG) and Spark Ablated Gold nano-particle size distributions measured by a DMS500 at different VSParticle setpoints

As can be seen, the generator was able to produce significant concentrations of spark ablated gold nanoparticles at sizes down to 7 to 10 nm, which is the correct size to be potentially useful for calibration of number counters and for use in equipment penetration efficiency studies. Also, it was seen that particles produced with graphite electrodes were in the size range 17 to 100 nm, which is representative of aircraft soot and again potentially useful for calibrating number and sizing particle instruments. In addition, the larger particle sizes (i.e., akin to particle mass) may be of use as a surrogate source for the calibration of carbon-based real-time mass instruments. Note that the internal structure of the carbon particles produced by the graphite electrodes was not investigated as part of this study, and may be amorphous, graphitic, or somewhere in between. For ease of terminology, the particles produced using the graphite electrodes will be referred to as Spark Ablated Graphite (SAG) throughout this document but do not necessarily represent pure graphite particles as measured. Future studies could use surface Raman spectroscopy and transmission electron microscopy to assess the internal structure of these carbon particles.

Table 4: Summary of VSParticle set points used in the trials

Test point	Electrode Material	N_2 flow (LPM)	Voltage (kV)	Current (mA)	Geometric Mean Diameter (nm)	Geometric Standard Deviation	Total number concentration (#/cm3)
Gr1	Graphite	10	1.3	10	22.4	1.66	2.85E+07
Gr2	Graphite	15	1.3	10	20.3	1.62	3.30E+07
Gr3	Graphite	10	1.3	8	20.3	1.63	2.99E+07
Gr4	Graphite	3	1.3	8	39.7	1.73	7.85E+06
Gr5	Graphite	1	1.3	10.4	72.0	1.85	1.06E+06
Go1	Gold	5	1.3	10	10.0	1.37	1.64E+07
Go2	Gold	15	1.3	10	7.7	1.35	8.91E+06

4.2. Catalytic Instruments Silver Particle Generator (SPG)

Catalytic instruments have developed and released a new Silver Particle Generator (SPG) which is based on the evaporation and condensation principle and shown in Figure 18. A loan instrument prototype was kindly made available to the SAMPLE IV consortium, by the instrument OEM, to trial as a particle source towards improved calibration method for VPR particle penetration and CPC counting efficiency. Using different furnace

temperatures, it is claimed to generate stable aerosols at concentrations of up to 500,000 particles/cm^3 in the 3 to 70 nm particle size range.

Figure 18: Photograph of Catalytic Instruments Silver Particle Generator (SPG) during trial

As seen in Figure 19, a range of particle sizes were achieved during the demonstration testing, with the GMD ranging from 6 to 18 nm and at high number concentrations. This particle size range is very relevant for CPC efficiency and VPR (small particle size) penetration calibrations.

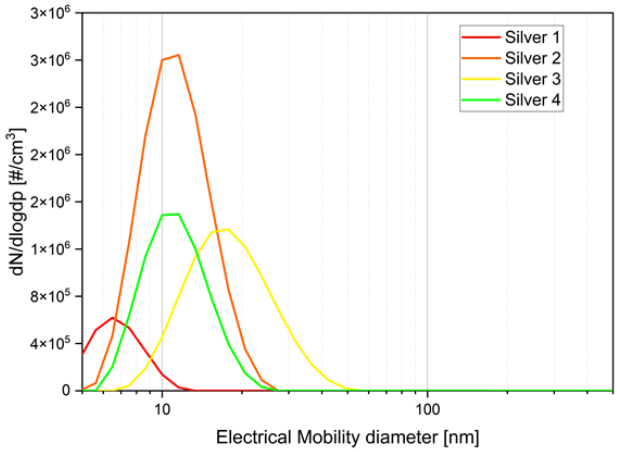

Figure 19: Silver particle size distributions measured by a DMS500 at different SPG set-points

4.3. Nebulised nanoparticles

A Topaz atomizer aerosol generator ATM 226[6] was used to produce a range of aerosol by nebulising suspensions (Carbon Black Powder, 'scraped' aircraft soot, Silica, and gold nanoparticles) and NaCl solutions (salt). The Carbon Black nanopowder was purchased[7] and suspended in ultrapure water by means of sonication, which was then nebulised for measurement, which is referred to as Nebulised Carbon Black (NCB) in this study. Some Carbon Black powder was also hydrogenated, prior to suspension, by being placed in a quartz tube furnace and heated to 600 °C under a hydrogen gas flow. This was done in an attempt to remove surface bound oxygen. The salt solution corresponds to a 0.9% w/v NaCl solution. Nebulised silica and gold suspensions, which were also tested, are discussed in more detail in Section 6.1. Example particle size distributions produced by NCB and salt can be seen in Figure 20.

[6] https://www.topas-gmbh.de/en/products/generation/product/atm-226
[7] https://www.nanoshel.com/product/carbon-black-nanopowder/

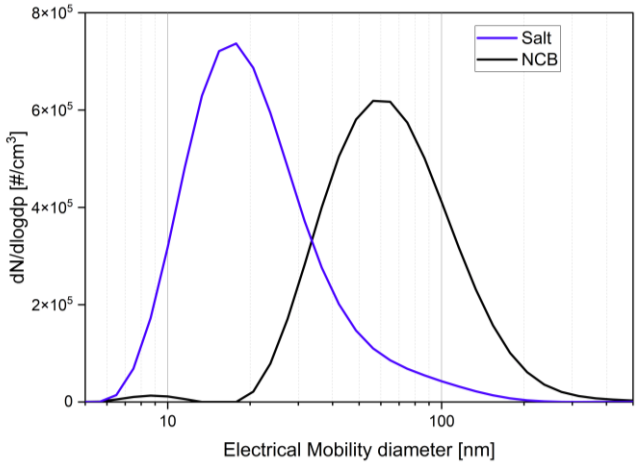

Figure 20: Nebulised Carbon Black (NCB) & Salt (NaCl) particle size distributions measured by a DMS500

4.4.GTRC's High Pressure Combustor Rig Design

4.4.1. High Pressure Optical Chamber (HPOC)

The HPOC is the central pressure-containing apparatus of the GTRC's High Pressure Combustor Rigs. The HPOC allows both axial and radial visual access to the burners and operational flames within it. Designed for pressures and preheat air temperatures of 16 bara and 573 K respectively, the HPOC is 0.716 m in length, with an inside diameter (ID) of 0.315 m. A thermal barrier coating has been applied along the entire ID of the HPOC to protect the stainless-steel casing from excessive temperatures during combustion experiments.

A working drawing and photograph of the HPOC are shown in Figure 21. During combustion experimentation, the flame is monitored remotely via HD cameras through a radial window, and aids in the visual confirmation of flame phenomena such as flame stability and combustion can thermal distribution.

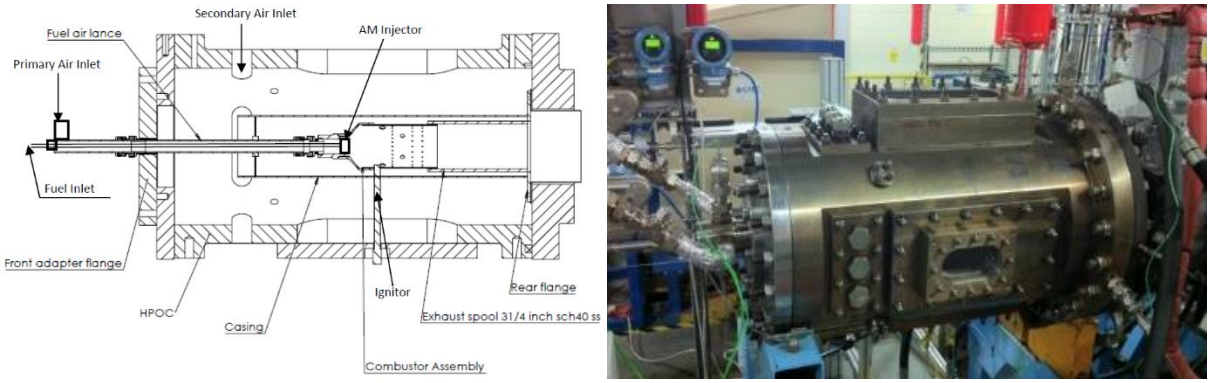

Figure 21: Drawing and Photograph of HPOC

4.4.2. Rich Quench Lean (RQL) combustor rig

A Rich Quench Lean (RQL) combustor rig was developed for use in the H2020 CLEANSKY2 funded RAPTOR programme based on recommendations presented in the literature[8,9,10] which was mounted within the HPOC. To introduce the fuel to the combustor a pre-filming air blast atomiser, designed using the Parker Hannifin

[8] Simmons, H.C. et al. 1975. AIR-ATOMIZING FUEL NOZZLE 3,980,233 [Patent].

[9] Stöhr, M. et al. 2019. Time-resolved study of transient soot formation in an aero-engine model combustor at elevated pressure. Proceedings of the Combustion Institute 37(4), pp. 5421–5428. doi: 10.1016/j.proci.2018.05.122.

[10] Makida, M. et al. 2006. Preliminary experimental research to develop a combustor for small class aircraft engine utilizing primary rich combustion approach. ASME Turbo Expo 2006 , pp. 1–8.

Corporation concept, has been successfully demonstrated as capable of producing a representative combustion source at low power conditions (125kW). The atomiser was manufactured using AM (Additive Manufacturing) techniques[11], adopting aspects of fuel nozzle design considerations, including swirl angles. Photographs of the RQL combustor before final assembly in the HPOC and mounted in the HPOC during combustion testing are presented below in Figure 22.

For this study, the RQL was configured for high repeatability and precise control over fuel and air flows, this was achieved using three high precision Emerson Coriolis MFCs, controlling three independent air lines and using a high precision Bronkhorst coriflow, magnetically coupled variable speed gear pump, to deliver set fuel flows. Fuel and airflow preheat temperatures were also independently maintained using water and electric heating systems. Different fuels with various GTL (Gas-to-Liquid) blends with Jet A were tested.

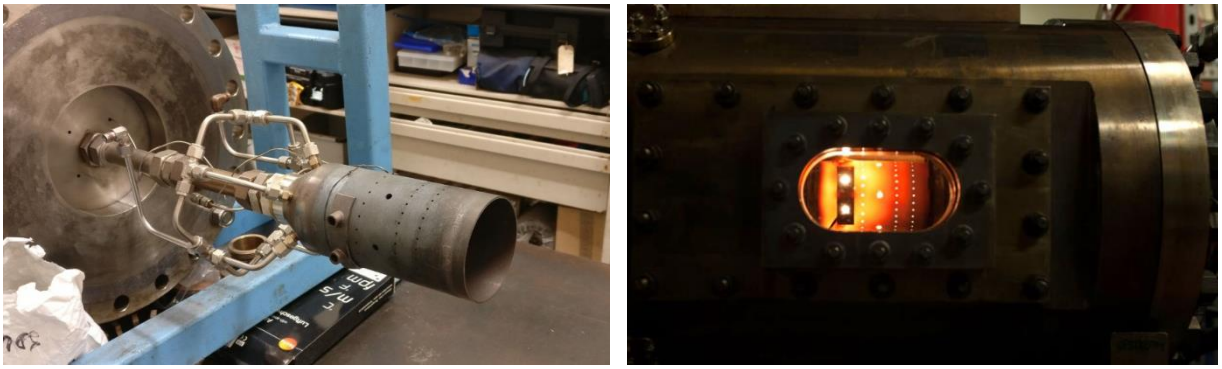

Figure 22: Picture of the RQL combustor during assembly and mounted in HPOC during combustion testing

5. Particle Mass, Number and Size instrument intercomparisons using novel particle sources

5.1. Experimental setup

The experimental setup for particle mass, number and size intercomparison can be found in Figure 23, Figure 24 and Figure 25 respectively. For all three experiments, A PALAS VKL10E was used to dilute and dry the aerosol followed by a Grimm 4-way flow splitter (critical orifice removed to allow significant flowrate without high pressure drop) to all the analysers. Conductive silicone tubing was used to connect the diluter to the splitter and to the analysers. It is noted that it was not always possible to ensure the tube length and flowrate to all analysers was precisely identical, however the particle loss differences were predicted to have a negligible impact (<1%). Leak/contamination checks were also performed before and after the experiments by placing a HEPA filter at the inlet of the diluter and checking all analysers measured zero particles.

For the number intercomparison, a DMS500 was used to measure the particle size distribution in parallel with an APC for comparison, and the UoM DMA was used to compare the two UoM CPCs (only labelled as “SMPS UoM” in diagram).

For the size intercomparison, the two DMS500 were equipped with their 5m integrated sample conditioning & dilution sample lines, which for this experiment were not heated and did not utilise the dilution stage.

[11] Crayford et al. 2019. Manufacture, characterization and stability limits of an AM Prefilming air-blast atomizer GT2019:91624

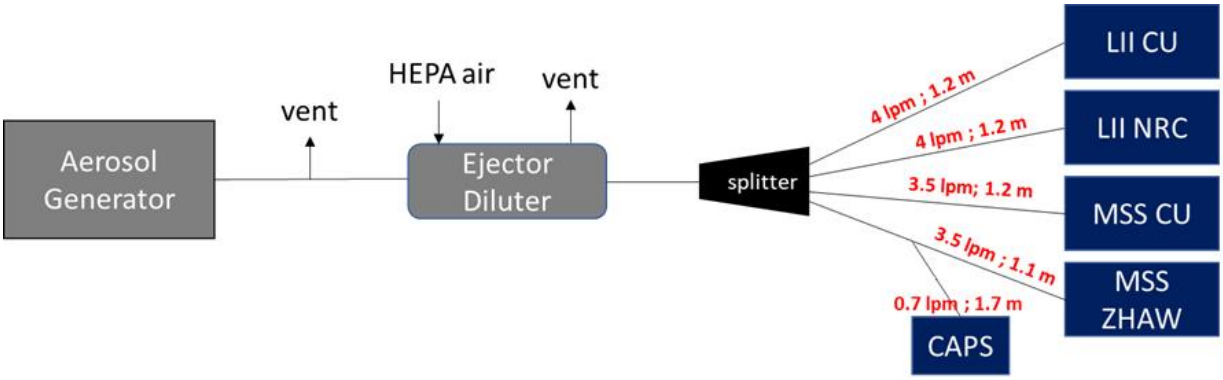

Figure 23: Diagram of the mass instrument intercomparison setup

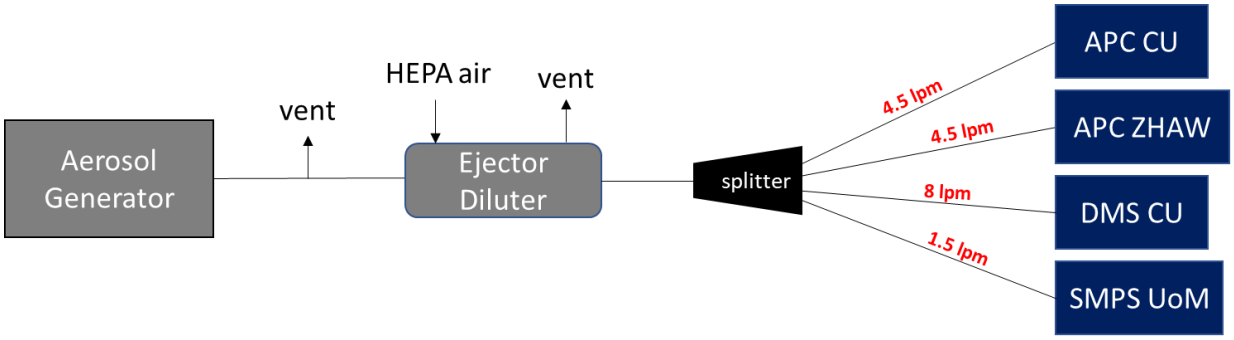

Figure 24: Diagram of the number instrument intercomparison setup

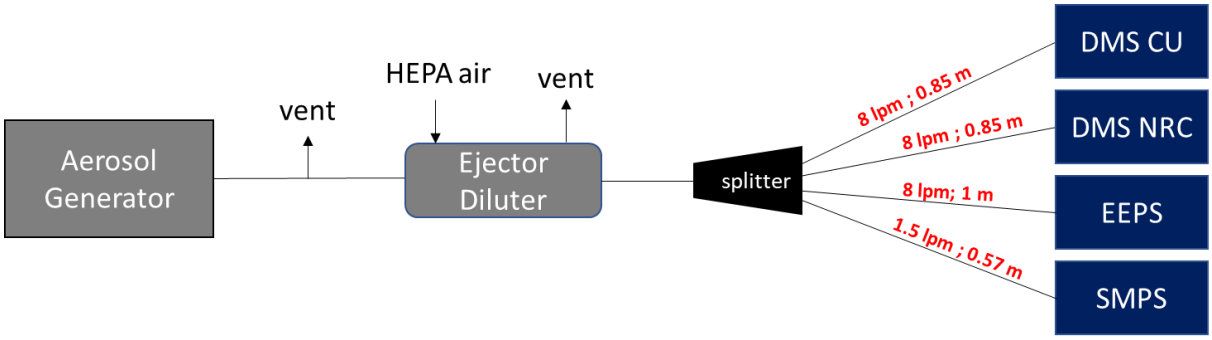

Figure 25: Diagram of the experimental setup for the size instrument intercomparison

5.2. Mass intercomparison results

Five nvPM mass measurement analysers, namely the EUR system LII-300 (SN0435), the NRC LII-300 (SN0331), the EUR system MSS (SN273), the Swiss system MSS (SN1065) and a ZHAW CAPS (SN315001) which operates at a wavelength of 660 nm, were compared with different particle types generated by a VSparticle (Graphite electrodes) and a nebuliser (hydrogenated and non-hydrogenated NCB). The test points correspond to a 60-second average a stable condition.

It is noted that both MSSs were calibrated in parallel on the same propane burner source (Jing miniCAST 5201C) by AVL Graz in September 2020. Using a Rolls-Royce Gnome engine, the EUR system LII-300 was calibrated in March 2020 and November 2021 and the NRC LII-300 was calibrated in March 2020. The CAPS was originally equipped with a 530 nm LED and was rebuilt at Aerodyne in 2020 to the 660 nm wavelength. The CAPS was not calibrated according to SAE ARP6320.

5.2.1. Results of Graphite and Black Carbon Tests

The results of the mass intercomparison experiment using SAG from the VSparticle and NCB are shown in Figure 26 and Figure 27. The analysers were compared at mass concentrations ranging from ~20 to ~400 µg/m^3 corresponding to a GMD range of ~20 to ~70 nm. No direct particle size measurements were performed during this experiment, but a nominally identical experimental setup was used for the comparison of particle size analysers, see Figure 23 & Figure 25. Note that the GSDs of SAG generated at smaller PSDs were wider causing high mass concentrations. For the NCB, the GMD stays constant with concentrations controlled using dilution alone.

Firstly, Figure 26 shows, that both MSSs and LII-300s agree very well with themselves with an average difference of 0.9% between the two MSSs and 0.6% between the two LII-300s. On these particle sources, the LII-300s generally reported a higher mass than the MSSs which was on average 16% in the case of SAG, and circa 30% for the NRC LII-300 in the case of the NCB sources. This difference is likely due to a difference in particle absorption properties but could also partly originate from the fact that the MSSs were calibrated in parallel on a mini-Cast source while the LII-300s were calibrated on a different particle source, a Gnome engine (also at different times). It is also noted that the percentage difference increased with decreasing mass for the NCB source, suggesting a potential zero offset for one or more of the instruments. The eBC instruments, namely the MSS and the PMssa CAPS, using a MAC[12] of 6.3 g/m^2, agreed within 1.8% of the MSS mean between 50-110 µg/m^3 but appeared to report increasingly lower concentrations compared to both the LII-300 and MSS (up to 13% lower than the MSS for TP1) as concentrations increased at mass loadings > 200 µg/m^3. Consulting the CAPS manufacturer literature, Aerodyne quote a measurement range of 0-1000 Mm^{-1}, which equates to approximately ~130 µg/m^3, hence this observation is consistent with these reported figures. It is noted that the CAPS data was corrected to STP (correction factor ~1.09) to afford a direct comparison with the other mass analysers all reporting at STP.

Comparing the error bars which highlight deviations over the 1-minute sampling average, it is noted that there appears to be higher scatter observed by all analysers whilst using the VSParticle, indicating it was a less stable source that the NCB in this experiment.

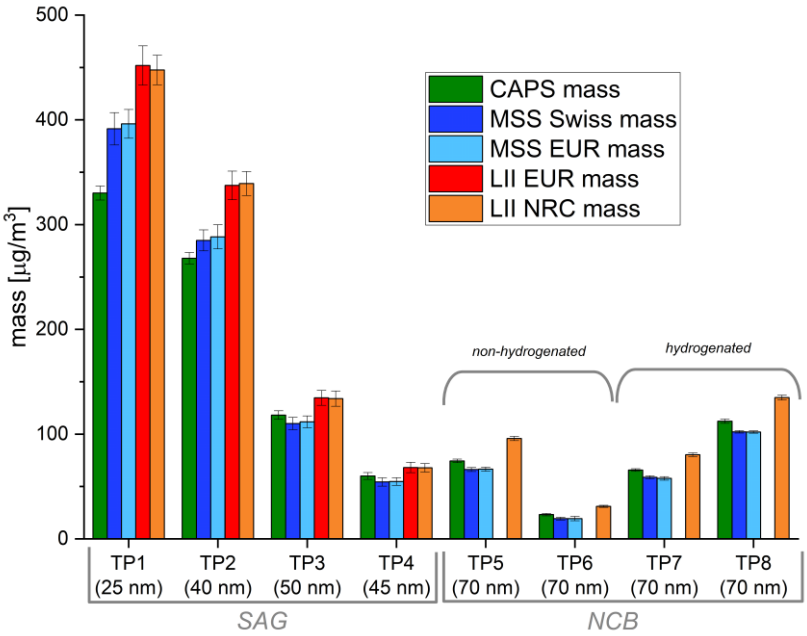

Figure 26: Bar chart results of the mass intercomparison experiment (error bars represent +/- 1 standard deviation

[12] T.C. Bond, R.W. Bergstrom, Light absorption by carbonaceous particles: An investigative review, Aerosol Sci. Technol. 40 (2006) 27–67. https://doi.org/10.1080/02786820500421521.

Figure 27 further highlights the above findings, showing that the MSSs and LII-300s agreed with themselves, with a bias between the LII-300s and the MSSs across all concentrations and sources, more so with NCB. It also shows that the CAPS deviated above the MSS at concentrations below 50 µg/m^3 and below the MSS at concentrations above 100 µg/m^3. This observation is indicative of a nonlinearity between the CAPS and MSSs, with a crossover at mass concentrations >125 µg/m^3 (close to the quoted max CAPS measurement range of 130 µg/m^3 quoted above). It is also noted that only SAG is measured at these higher concentrations hence particle morphology could also be impacting this observation. Finally, it is seen that all mass measurements agree within 20% of their mean, except for the NRC LII-300 on NCB. It should be also mentioned that NCB hydrogenation does not appear to have any impact on the various mass analysers trialled, given there are no observable differences TP5-6 (non-hydrogenated NCB) and TP7-8 (hydrogenated NCB).

It is noted that the EUR LII-300 was inadvertently put in high-sensitivity mode, which had not been calibrated, from TP5 onwards. This resulted in under-reporting of the mass for the NCB test points which is why its data has been removed from TP5-TP8 in Figure 26. Normalising the EUR High Sensitivity LII-300 signal output to the NRC LII-300 resulted in similar observed trends.

Given that CAPS and MSS measure forms of equivalent BC (eBC) and the LII-300 measures refractory BC (rBC) it is unsurprising, that all the instruments are reacting differently to these different carbon particles, which are likely to have different carbon bonding/graphitisation and hence (MAC) absorption properties. Similarly, the LII-300 fluence was left at the optimum for aircraft soot (instead of optimising for these specific particle sources) during these studies, which would have impacted the witnessed results. Recent work[13] has also provided evidence of a size dependent MAC that would directly affect both eBC instruments if the size of the graphite and NCB particles is in the range where MAC is varying. This would contribute to the differences observed between the CAPS and MSS in comparison to the LII-300.

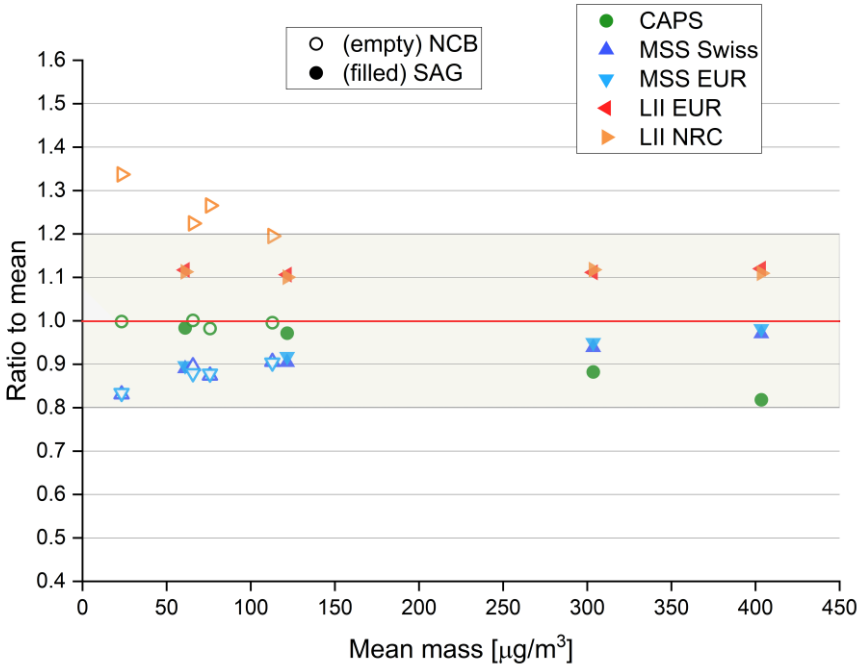

Figure 27: Ratio of the different mass measurements with regards to their mean

[13] Corbin et al., "Size-dependent mass absorption cross-section of soot particles from various sources," accepted for publication in Carbon (2022).

5.3. Fluence measurements of novel mass sources

The use of Laser-Induced I(LII) as a technique to measure black carbon, soot, and nvPM was developed and refined over a few decades. LII is performed by rapidly heating the particles to near sublimation temperatures (~4000 K) with a short pulse duration laser and measuring the incandescent signals emanating from the very hot particles. The mass concentration is determined from these signals. This is the operating principle of the Artium Technologies LII-300 instrument. For a given particle source, the signal produced by LII can be dependent upon the laser fluence (energy per unit area of the laser light beam) at high fluences due to sublimation of the particles, and at low fluences due to insufficient heating of the particles. A recent study[14] showed that there is a wide range of moderate laser fluences where the signal is independent of the laser fluence (plateau region), where the resulting mass concentrations are constant, regardless of laser fluence. Demonstrating the mass concentration response to varying the laser fluence from low values to high values is known as a *fluence sweep*. In the study, it was shown for a number of sources (engines and combustion rigs) and fuels (Jet A-1, gasoline, and diesel), the fluence sweeps were self-similar. The optimum range, where the mass concentration was invariant as the fluence was changed, was wide, but also was at slightly different fluences for different sources, operating conditions, and fuels. These differences in the fluence at which the optimum range occurs is because the physical and composition properties of the particles may vary with the source, the fuel, and the source operating condition. Changes in the properties such as light absorption and organic coatings may affect the amount of laser fluence required to achieve incandescent temperatures. As a result, the fluence may be optimised for a range of different sources, operating conditions, and fuels to which an LII instrument is anticipated to be applied. For aircraft engines, the source and fuel are going to be similar (gas turbine engine and Jet A-1), and the operating conditions, from idle to full thrust, will be the most significant variable affecting the properties and therefore the required fluence. The Artium LII-300 has its laser fluence set to be in the optimum range for a wide range of particle types, but of course has not been validated for all particle source types. This parameter may be adjusted to be in the desired range by experts, with the adjustment not available to non-expert users.

This current study is investigating 'novel' sources for the calibration of the mass concentration instruments, including the LII-300. To fully understand the response of the LII-300 in this study, it is important to ensure that it is in a range of fluence when the mass concentration is invariant with fluence so that small perturbations in the laser fluence do not affect the measurement of mass concentration. Thus, performing fluence sweeps on the LII-300 helps assess the optimum fluence for each particle source and helps inform whether the source has potential to be a representative calibration source in comparison to the Diffusion Flame Combustion Aerosol Source (DFCAS) typically used (Rolls-Royce Gnome engine). Fluence sweeps also aid in assessing potential differences witnessed between the eBC analysers and rBC analysers on different 'novel' particle materials. Fluence sweeps were performed for the different novel carbonaceous particle types using the NRC LII-300 instrument.

The laser fluence is controlled by adjusting the Q-switch delay, with longer Q-switch delays corresponding to lower laser fluences, less laser energy, less heating of the particles, and lower particle peak temperatures. The Q-switch delay was varied from 135 to 265 µs in increments of 5 or 10 µs and a measurement period of 10 seconds was taken at each Q-switch delay value. The Q-switch delay value of 135 µs was used as a reference to account for variations in the source stability and was repeated four times for each fluence sweep performed.

The results are shown in Figure 28, with the lines corresponding to a 4th degree polynomial fit to the measurement data for the various particle types investigated. The polynomial fits to the measurement data shown in Figure 28 are peak normalised for comparison purposes. The general trends for all sources are similar. Every source has a region with a plateau at the peak mass concentration where the mass concentration is invariant with Q-switch delay (and therefore with laser fluence), as described above. As an example, for the 21 nm GMD SAG produced by the VSParticle (light grey solid line), the mass concentration is

[14] Yuan, et al. Measurement of black carbon emissions from multiple engine and source types using laser-induced incandescence: sensitivity to laser fluence, Atmos. Meas. Tech., 15, 241–259, https://doi.org/10.5194/amt-15-241-2022, 2022.

flat and uniform from 135 µs to 180 µs (representing a wide range of laser fluence) with less than ±1% variation. This is the optimum region for operating the LII-300 instrument, as the instrument response will be insensitive to small changes in the laser fluence and in the particle properties.

However, concentrations lower than the peak may be observed for some particles at low Q-switch delays, where the laser fluence is greatest and these particles are showing evidence of sublimation (mass concentrations less than the peak value). The particles from 75% GTL (green dashed line) is one example demonstrating this, with 8% mass loss for Q-switch delays between 135 µs and 180 µs. These particles have an optimum Q-switch delay between 165 µs to 195 µs, where there is less than ±2% variation in the mass concentration.

At large Q-switch delays, where the laser fluence is the lowest, the concentrations for all particle types are observed to drop below the peak concentration observed in the plateau region. This happens at Q-switch delays greater than 195 µs for the particles from 75% GTL (green dashed line), NCB (hydrogenated – black dashed line) and NAS_{PW4000} (hydrogenated – orange dashed line), where there is more than ±2% variation in the mass concentration. Some types of particles exhibit almost identical fluence sweeps to each other, such as the NCB (hydrogenated – black dashed line) and NAS_{PW4000} (hydrogenated – orange dashed line), indicating they may be interchangeable. A particle source with a fluence sweep behaviour identical to that for nvPM from a gas turbine engine would be an ideal candidate for calibration of LII-300 instruments.

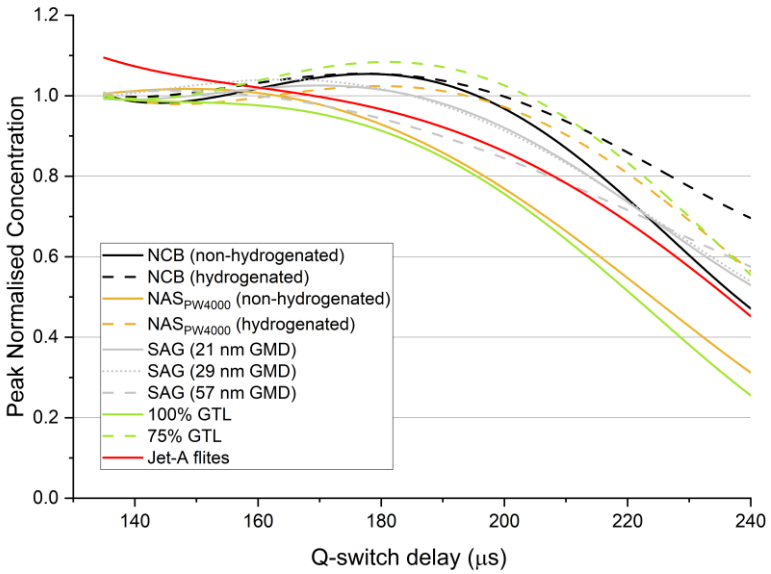

Figure 28: Fluence sweeps for various carbonaceous particle types, illustrating the optimum range of Q-switch delays for the LII-300 instrument. Varying Q-switch delay varies the laser fluence, which in turn may affect the reported mass concentration

Following the procedure demonstrated[14], some of the fluence curves (previously shown in Figure 28) have been shifted in Figure 29 on the Q-switch delay axis to illustrate the similarity in shape of the fluence sweep results for all particle types investigated. The degree of this shift is dependent upon the differences in physical properties of the particle types, suggesting lower absorption by some particles, or increased presence of VOCs, or other aspects that affect the magnitude of the laser fluence that is optimum in order to achieve the plateau region. Previously NRC had determined that the optimum fluence for this LII-300 instrument using the Gnome engine at high power as a calibration particle source was at a Q-switch delay of 180 µs. Several of the particle sources also had this Q-switch delay as their peak normalised concentration and thus optimised fluence, without requiring a shift, namely NCB (hydrogenated), NCB (non-hydrogenated), NAS_{PW4000} (hydrogenated) and combustor rig operating on 75% GTL. This implies these particles may be good candidates for calibration of the LII-300 instruments.

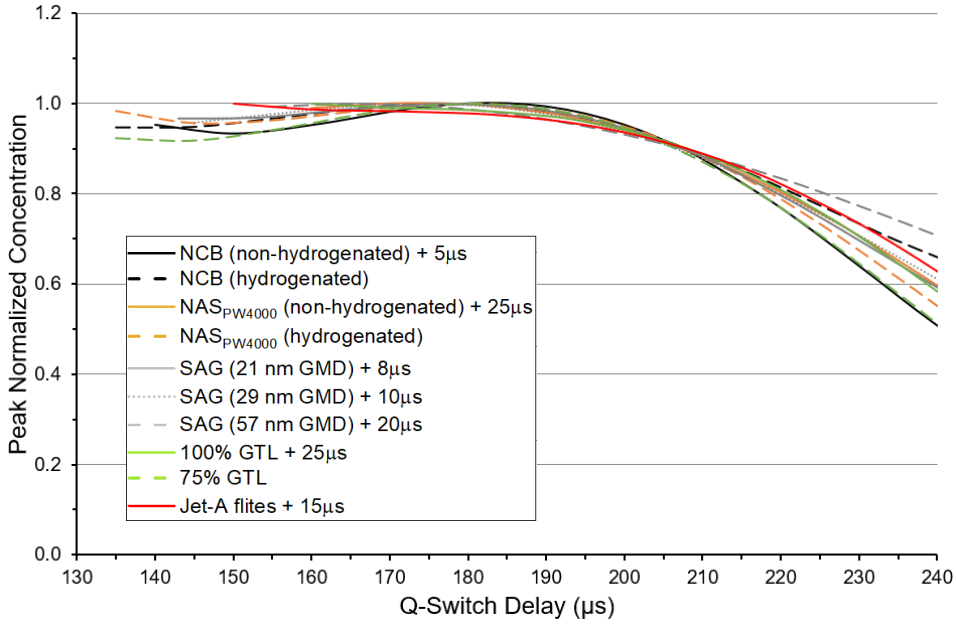

Figure 29: Shifted fluence sweeps for various carbonaceous particle types, illustrating the self-similarity of the fluence sweep behaviour

The tested particle sources that required fluence shifts (as shown in Figure 29) are potentially less suitable as a source for calibrating the LII-300 for measurements on the Gnome at high power. However, the most recent fluence sweep curve for this instrument (LII-300 SN 0331) suggests the data is relatively flat from 135 µs to 180 µs when using particles from the Gnome engine at high power and reaches a peak at 135 µs when the Gnome is a low power (idle). So, an optimum compromise Q-switch delay would be 135 µs for the Gnome covering the range of particles from low to high power conditions. In this case, a source that is relatively flat from 135 µs to 180 µs might be most suitable for calibrating this instrument for application to aircraft engines. Optimum sources for that application might include:

- Combustor rig - Jet-A
- SAG (21 nm GMD)
- SAG (29 nm GMD)
- NAS_{PW4000} (hydrogenated)

All these particle sources had less than ±2.5% variation from 135 µs to 180 µs. Hydrogenated NCB was only slightly more than ±2.5%, so could also be included.

Fluence sweep data was not able to be repeated for all particle sources due to time constraints and data was noisy due to fluctuations in the particle source concentration output. For future research, a constant mass reference and/or multiple repeats would help to reduce data variability and increase confidence in the selection of candidate novel particle sources from the perspective of determining the optimum fluence.

5.4. Number instrument intercomparison

The Swiss and EUR reference systems both utilise APC number counting units, which broadly comprise of a rotary dilution stage, evaporation tube, catalytic stripper, mass flow dilution stage and CPC. These two units were calibrated in parallel at AVL Graz in September 2020, for the H2020 RAPTOR research programme to understand uncertainty associated with calibration. During the December 2021 SAMPLE IV test campaign, the two APCs were compared using various particle sources including Spark Ablated Gold, SPG silver, SAG, nebulised salt, and NCB as described previously.

The range of aerosols techniques trialled afforded a GMD size range from ~ 7 to 70 nm, which is thought representative of the size of particles witnessed in modern aviation gas turbine exhaust. The inbuilt APC internal dilution factors (DF_2) were also varied from the minimum (PCRF ~ 100) to the maximum (PCRF ~ 1500) on given sources to understand the impact of dilution rate on uncertainty. It is noted that this experiment was performed in parallel with the CPC intercomparison experiment.

The first intercomparison results of the Swiss and EUR APCs are shown in Figure 30 comparing the ratio of relative reported number concentration plotted against both GMD (a) and CPC raw count (b).

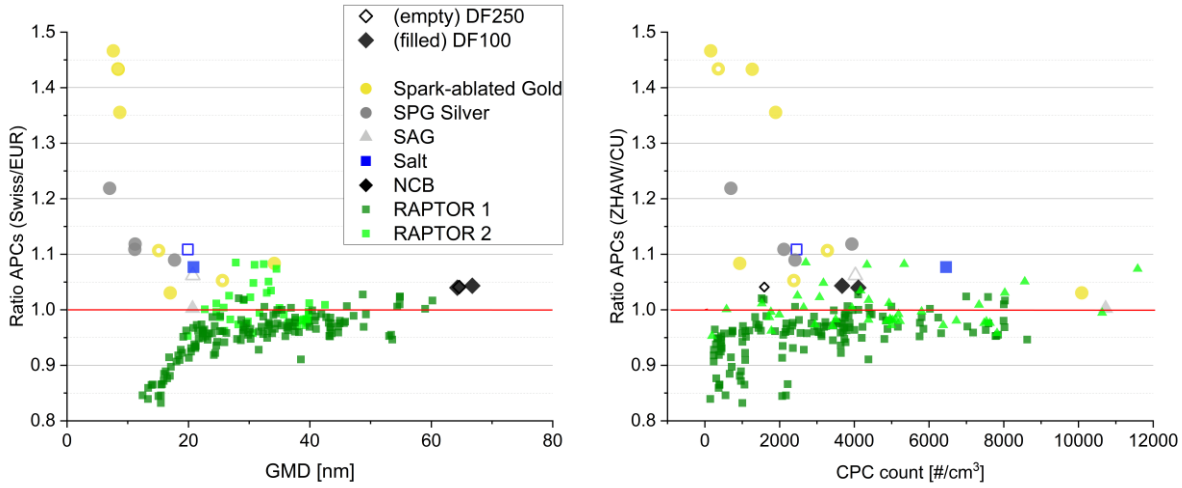

Figure 30: a&b: Ratio of the Swiss and EUR APCs against the GMD and EUR APC total CPC count respectively

As can be seen across all the laboratory generated test aerosols the Swiss APC reported > 5% higher number concentrations than the EUR APC, with the morphology of the aerosol not appearing to have a large influence on the relative difference. It is noted that above 15 nm (1000 #/cm^3) that a relative agreement of circa ~ 6.1% (average ratio 1.061) was observed. It is also noted in Figure 30, that the impact of using PCRF settings of either 100 or 250 (which are typical settings used in aviation engine testing) does not appear to affect the relative difference between the two APCs.

However, it is evident from Figure 30 a& b that the relative difference rises sharply towards the left- hand side of the graphs as a result of either the small particle size or the relatively low concentration of the particles. The relatively lower scatter of the Spark Ablated Gold particles from the apparent trend may suggest that it is the size, which is the major influence of this disparity. However further experiments varying concentration at different small sizes would be required to validate this hypothesis. Comparing the laboratory generated test aerosol data it is noted that this trend is in contradiction to the relative differences observed between the measured nvPM of the EUR and Swiss systems during the first H2020 RAPTOR RQL test conducted December 2020. As can be seen by the green data points in Figure 30 higher concentrations of smaller particles are reported by the EUR APC compared to the Swiss APC when measuring combustor rig soot at the end of their relative sampling systems.

Consulting the previous calibration certificates of the two units (see Appendix), which were undertaken 13 months prior to this experiment, it is noted that the CPC cut-off is very similar for both units as would be expected after parallel servicing. Interestingly, the Swiss VPR had higher particle loss at small sizes at the time of calibration (3% higher at 15 nm and 1% higher at 30 nm), which is in contradiction to the data observed in this test.

Figure 31 shows the impact of using high PCRF settings on the two APCs. It is seen that when comparing the relative difference in reported number concentration at rising dilution factors (PCRF settings) for nebulised Black Carbon (1 mg/ml non-hydrogenated, circa 65 nm), the relative agreement gets worse at higher PCRF (DF2) settings.

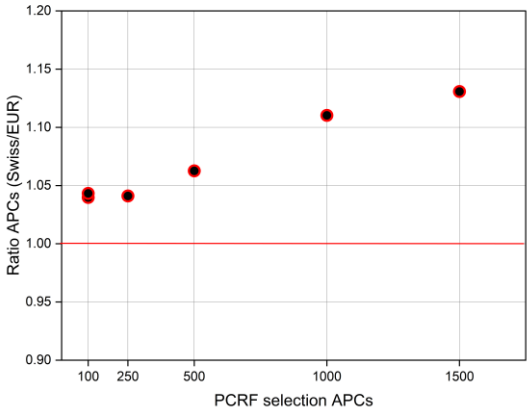

Figure 31: Ratio of the Swiss and EUR APCs against the selected PCRF (~DF2) when measuring NCB

As can be seen in Figure 31, and in agreement with earlier discussions of Figure 30, relatively good agreement is observed for the 100 & 250 PCRF (DF2) set points with it again noted that typically PCRF settings of 100 & 250 are used during engine certification testing.

However, the relative agreement of the two APC gets progressively worse at higher PCRF settings, rising from 4% differences at the 100 & 250 settings up to 12.5% differences at the maximum 1500 setpoint.

5.5. VPR instrument intercomparison

To assess whether the relative differences in the reported number concentrations from the APCs were associated with the VPR, following completion of the combustor rig experiments, penetration experiments were undertaken using different aerosol sources namely Spark Ablated Gold, SPG silver and SAG which were size selected using a DMA. The setup of this experiment is shown in Figure 32.

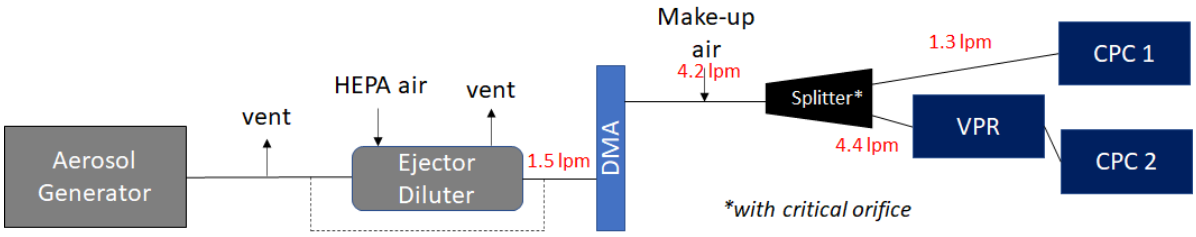

Figure 32: Diagram of the VPR penetration measurement setup

It was first necessary to intercompare 2 nominally identical TSI 3756 CPCs (D_{50} 2.5nm) owned by UoM, to perform real-time size dependant penetration experiments down to particle sizes of 5nm. These CPCs were then subsequently used to measure concentrations of the different aerosols pre and post the EUR and Swiss VPR's.

Comparisons of the two CPCs were performed using Spark Ablated Gold, and SAG from the VSParticle and SPG Silver with the relative differences highlighted in Figure 33, Figure 34 and Figure 35 respectively.

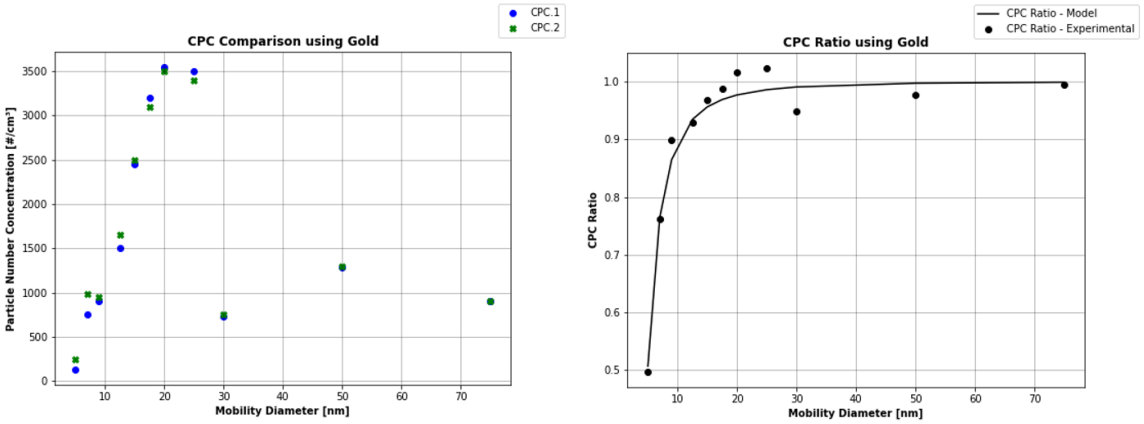

Figure 33: (a&b): CPC intercomparison using size selected Spark Ablated Gold highlighting relative difference in reported number concentration and ratio of response respectively

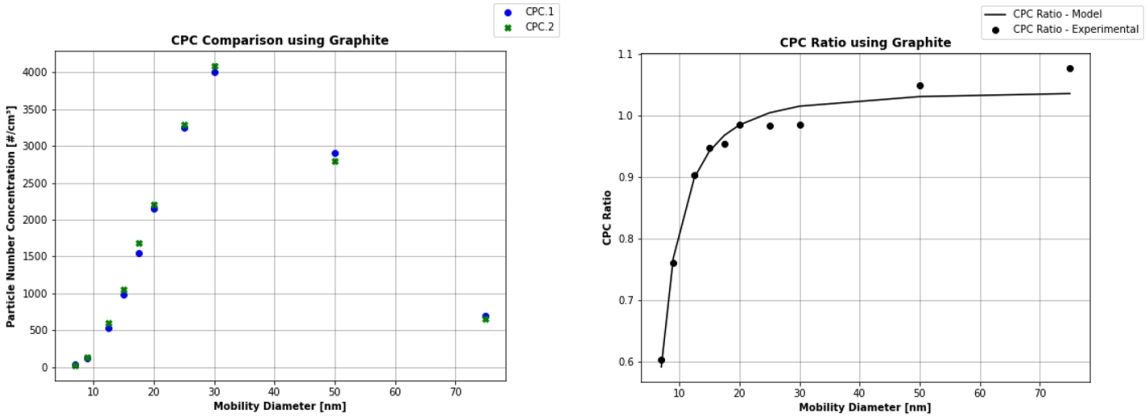

Figure 34: (a&b): CPC intercomparison using size selected Spark Ablated Graphite (SPG highlighting relative difference in reported number concentration and ratio of response respectively

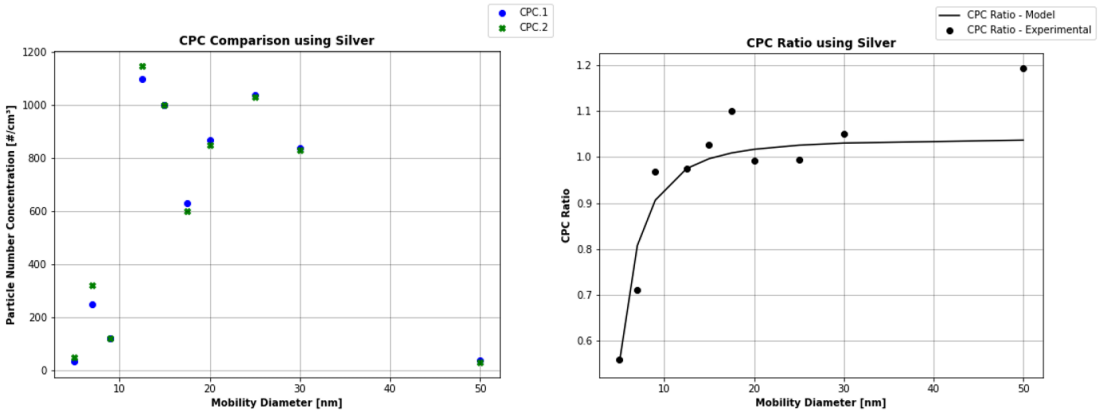

Figure 35: (a&b): CPC intercomparison using size selected SPG Silver highlighting relative difference in reported number concentration and ratio of response respectively

It is noted in Figure 33-Figure 35 that unfortunately it was not possible to maintain the same concentrations, and therefore differentiate size-dependent and linearity effects, across all size ranges using the spark ablated gold and SAG aerosols. Significantly lower concentrations of aerosol were emitted by the VSParticle at different particle sizes and there is significant loss of the smallest particles, which are hard to produce at high concentrations, in the size selecting DMA.

Similarly, for the SPG due to time constraints, it was not possible to change the furnace temperature numerous times to 'tune' the size of particles to select, again leading to a variation in concentrations across different selected mobility diameters.

As can be seen in Figure 33b-Figure 35b, it appears for all three aerosols good agreement between the two CPCs is not reached till > 15nm, which is surprising given the D_{50} of the units is 2.5nm. Note that particle number concentrations were not consistent across the size range.

The penetrations of the EUR (VPR1) and Swiss (VPR2) APC VPRs, measured with two CPC's up and downstream of the VPRs respectively, are presented below in Figure 36. As can be seen it appears for both systems the measured penetrations are 20% lower than would have been expected given the certified calibration values (see Appendix) and values reported in the H2020 Raptor programme. It is thought that the observed difference in penetration may be attributed to uncertainty associated with the relative counting efficiencies of the two CPCs at different sizes for specific test aerosol material, which highlights that further definition of the method for the derivation of penetration of particles through a VPR may be required, particularly if surrogate particles are to be used.

To improve VPR penetration uncertainty understanding, further work was undertaken concerned with the uncertainties in penetration measurement[15].

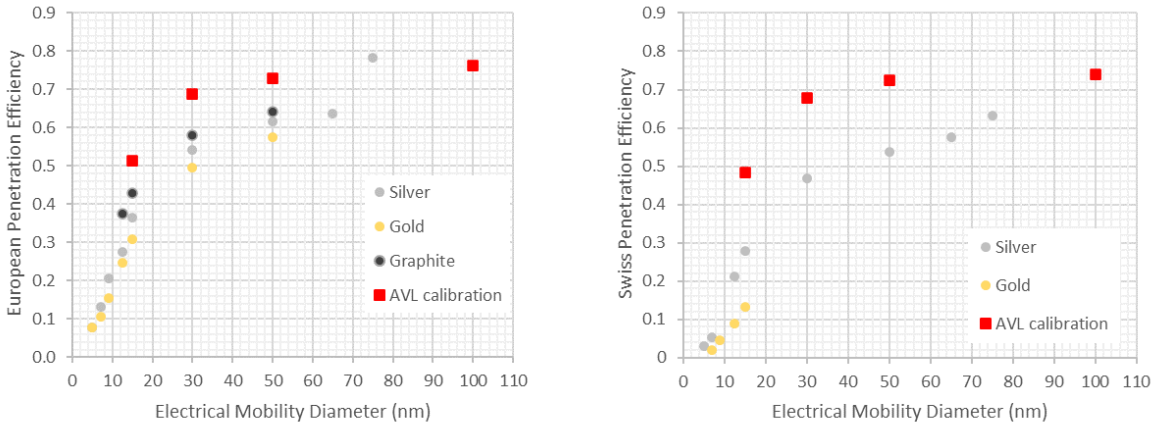

Figure 36: (a&b) Measured penetration efficiencies of the EUR and Swiss VPRs respectively, using SPG Silver, Spark Ablated Gold and Spark Ablated Graphite (SAG)

Further investigation of this penetration data highlighted that two orders of magnitude differences were observed in particle number concentrations before and after the VPR. Accounting for the dilution factor of circa 70 coupled with the diffusion and thermophoretic particle loss, highlighting the importance of relative accuracy of particle counting (at small particle size) for the CPCs used to measure the penetration. Differences in morphology of these laboratory generated aerosols compared to the CAST aerosol and RQL combustor rig aerosol used in RAPTOR are thought to have negligible effect on VPR penetration as most of the loss is attributed to diffusion at these small particle sizes, which directly relates to mobility size.

In an attempt to reduce the CPC measurement error towards understanding the relative penetration of the two VPRs, the relative penetrations (measured using exact same CPCs with same relative differences using the silver particles which afforded a concentration of >5000 particles/cm^3) were predicted by normalising the EUR and Swiss VPR penetration efficiencies to one and other with the data presented in Figure 37.

[15] Further information found in SAMPLE IV Deliverable Report 3

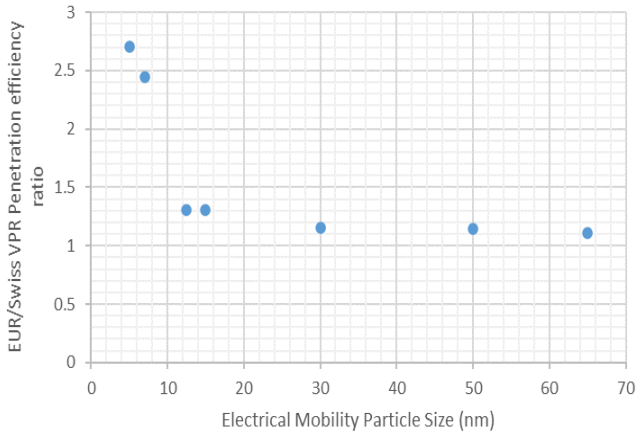

Figure 37: Relative penetrations of EUR and Swiss VPRs for different particle sizes using the silver aerosol

As is seen, by ratioing the penetrations against one and other, it appears that the Swiss systems VPR has a lower penetration efficiency than that of the EUR VPR particularly at the smallest sizes. It is noted that the lower penetration efficiency of the Swiss VPR displays the same trend as was witnessed in both the calibration certificates (Appendix) and previously reported differences of the full APCs (VPR & CPC) witnessed in the first H2020 RAPTOR test, noting that the witnessed difference is higher in this case. However, given the trend for the APC intercomparison shown above (Figure 30), which indicated a higher reported number concentration in the case of the Swiss APC, this would suggest that the CPC counting efficiencies at the lowest sizes are significantly different, with the Swiss CPC counting more efficiently than the EUR CPC at sizes less than 20nm.

It is observed that variations in counting efficiency at small GMDs in some circumstances can increase the uncertainty in reported EIs. This highlights, that understanding how CPCs 'drift' in terms of their linearity and counting efficiency over a calibration period of 12 months is needed. Therefore, 'as found' calibrations which determine changes to the CPC counting performance brought about by factors such as wick degradation and/or changes in saturator temperatures prior to 12-month service and calibration, were deemed necessary by SAE E31. Given the predictability of engine testing dates and the lengthy calibration process (scheduling, shipping, calibration, shipping…), there have been occasions when engine test campaigns were conducted using analysers that are slightly beyond their recommended calibration schedule. In such scenarios 'as found' calibrations are critical in understanding any additional uncertainty that may have occurred. In recognition of this the SAE E31 have informed ICAO CAEP WG3 of potential uncertainties associated with 'past due' calibration testing, which is anticipated may be documented in future SAE Aerospace Information Reports (AIRs). In the case of mass measurement, it is noted that the uncertainties associated with 'past due' calibrations will need to be considered differently than those of number counting CPCs, given it is perceived that the relative uncertainty of the annual (NIOSH 5040) mass calibration method is currently significantly larger than the drift of a mass instrument over the 12-month calibration period.

5.6. Size instrument intercomparison

Towards assessing the relative agreement of different real-time (fast) sizing instruments, currently being considered for use in the size dependent system loss correction of ICAO Annex 16 Vol II compliant nvPM systems, intercomparison studies were undertaken using a number of different aerosol sources on four particle size measurement analysers, namely the CU DMS500 (M44), the NRC DMS500 (M125), a loaned TSI EEPS (Model 3090), and the ZHAW SMPS (3082 classifier, aerosol neutralizer 3077A, DMA 3081 & CPC 3776).

These different analysers were compared using different particle types generated by the VSparticle (spark ablated Graphite (SAG) and spark ablated gold) and a nebuliser (hydrogenated and non-hydrogenated Nebulised Carbon Black (NCB)). The test points correspond to a 60-second average (i.e., 2 SMPS scans) on a stable condition. The particle size distribution properties (statistical GMD, GSD, total Number) were all derived using the same MATLAB code (see Appendix) to ensure direct comparability.

5.6.1. Size intercomparison results (using Spark Ablated Gold, SAG and NCB)

The results of the size intercomparison experiment are shown in Figure 38, Figure 39, and Figure 40 in terms of statistical GMD, GSD and total number for spark ablated gold, SAG and NCB respectively. Both spherical and soot inversion matrices were used for the DMS500s and the EEPS (the EEPS default inversion matrix wasn't investigated) with the SMPS distribution calculated using the standard AIMS inversion. It is noted that the time at which the different instruments were last calibrated and serviced varied significantly which may impact the results below; The EEPS was calibrated in July 2020, the CU DMS500 was calibrated in September 2020, and both the SMPS and the NRC DMS500 were calibrated/serviced in October 2021.

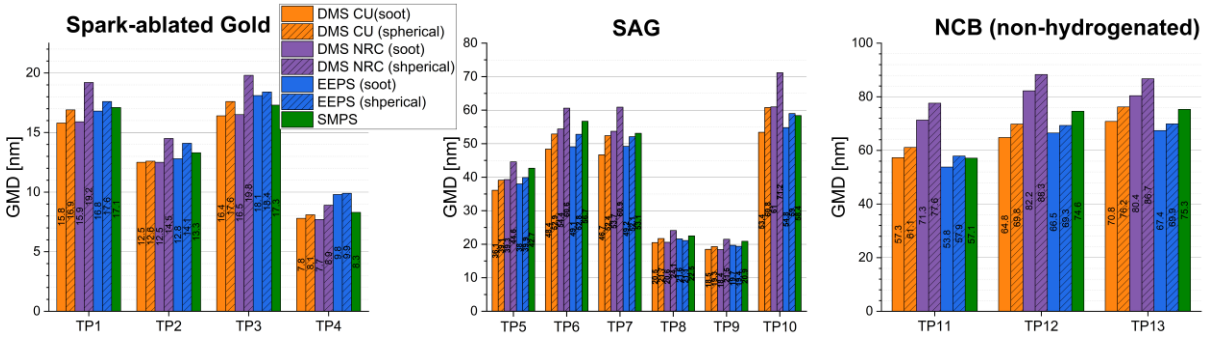

Figure 38: GMD measured by various analysers and inversion matrices for Spark Ablated Gold (left), Spark Ablated Graphite (SAG) (middle) and non-hydrogenated Nebulised Carbon Black (NCB) (right) (note TP4 gold – for the SMPS, the GMD, GSD and total number from the lognormal fit were used given only part of the distribution was measured)

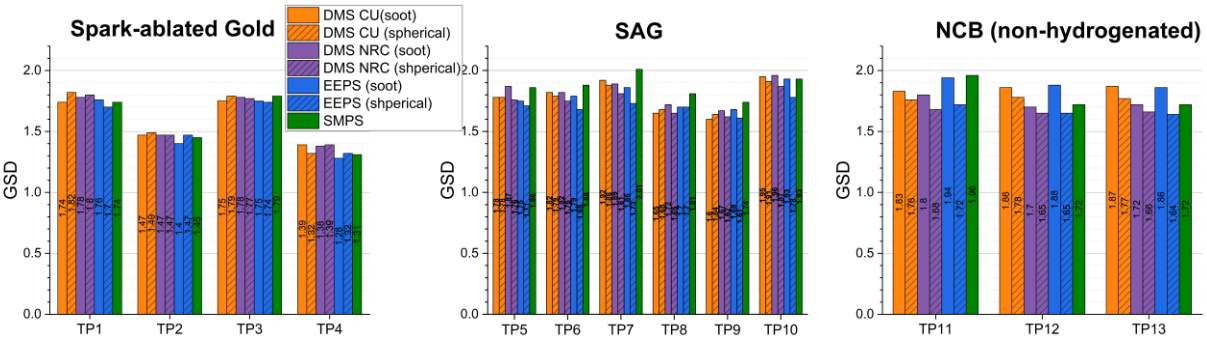

Figure 39: GSD measured by various analysers and inversion matrices for Spark Ablated Gold (left), Spark Ablated Graphite (SAG) (middle) and non-hydrogenated Nebulised Carbon Black (NCB) (right)

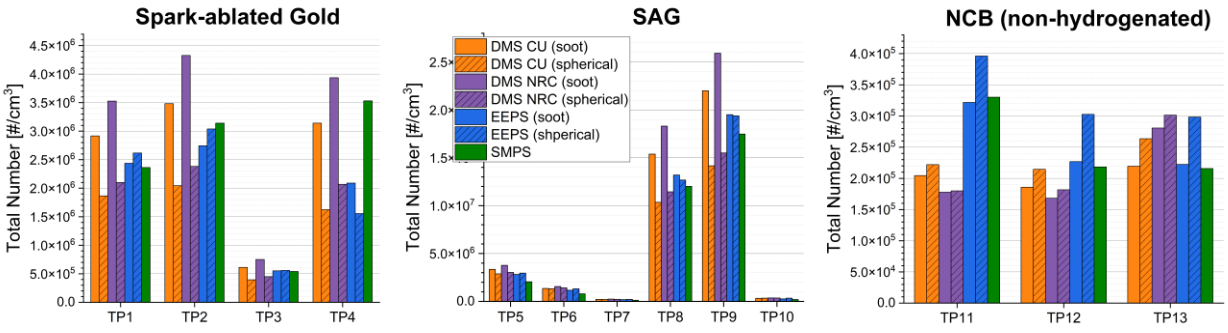

Figure 40: Total number measured by various analysers and inversion matrices for Spark Ablated Gold (left), Spark Ablated Graphite (SAG) (middle) and non-hydrogenated Nebulised Carbon Black (NCB) (right)

Summary statistics can also be found in Table 5, from which it can be seen that all analysers (and inversion matrices) agree within a coefficient of variation (i.e., standard deviation/average) of 8.3% for GMD across all test points and 3.4% for GSD within a size ranging from 8 to 75 nm and a number concentration ranging from 2E+05 to 2E+07 particles/cm^3. Slightly higher GMD and GSD variations are observed when measuring non-

hydrogenated NCB when compared with SAG or spark ablated gold, however it is noted that the NCB also produced the largest GMDs.

While the DMS500 reports the total number concentration at STP, the SMPS and EEPS report the data at the actual sample pressure and temperature. In the case of the SMPS, the correction also depends on the accuracy of the inlet flow measurement using the inlet impactor. The SMPS-reported total particle count is referenced to the inlet flow rate measured (or inserted manually in the scan settings). In this work it was assumed that the inlet flow measured using the impactor was correct and therefore STP correction was performed for both the SMPS and EEPS using the sample temperatures and pressures reported. The correction was on the order of 12-14% (i.e., correction factor of 1.12-1.14).

STP-corrected total number concentrations agree within a coefficient of variation of 20.4%, a higher variation than with GMD and GSD, however it is noted that some measured size distributions (e.g., TP4) were not fully captured by all analysers and that the total number derived from a particle size measurement is known to have a higher uncertainty than the GMD (e.g., Cambustion quotes a 10% uncertainty for size and a 20% uncertainty for number for a calibrated DMS500). The impact of adding a chemical drier in-line with the NCB was also investigated; It was found that it did not further reduce the relative humidity nor impact the measured particle size distributions (other than the expected higher diffusional loss), demonstrating that diluting with dry air alone is enough to fully evaporate the nebulised aerosol and maintain a low relative humidity.

Table 5: Average statistics of GMD, GSD & total number from the size intercomparison experiment

		Average GMD [nm]	CV [%]	Average GSD	CV [%]	Average Ntot [#/cm^3]	CV [%]
Spark Ablated Gold	TP1	17.0	6.7%	1.76	1.8%	2.55E+06	18.1%
	TP2	13.2	5.9%	1.46	1.8%	3.02E+06	20.3%
	TP3	17.7	6.6%	1.77	1.0%	5.51E+05	16.6%
	TP4	8.7	9.8%	1.34	3.2%	2.56E+06	33.8%
SAG	TP5	40.0	7.1%	1.79	3.3%	2.98E+06	17.6%
	TP6	53.6	7.9%	1.79	3.5%	1.28E+06	19.0%
	TP7	52.6	8.4%	1.87	4.7%	2.04E+05	18.4%
	TP8	21.7	5.8%	1.70	3.2%	1.33E+07	17.6%
	TP9	19.7	5.8%	1.65	3.0%	1.91E+07	17.4%
	TP10	59.8	9.6%	1.90	3.3%	3.18E+05	18.1%
NCB	TP11	62.3	14.0%	1.81	5.7%	2.62E+05	32.4%
	TP12	73.6	11.6%	1.75	5.3%	2.14E+05	20.9%
	TP13	75.2	8.9%	1.75	5.1%	2.57E+05	14.7%
Average CV all			8.3%		3.4%		20.4%

The full size intercomparison results are also presented in Figure 41 whereby the ratio between each size measurement (including different inversion matrices for the individual DMS and EEPS) and the average of all measurements at a given test point is plotted against mean for the mean GMD, GSD and N_{tot}. The observed ratios for GMD generally agree within 15%, except for the NRC DMS data processed using the spherical inversion. For GSD the ratios all agree within 8% and for total number within 60%. Figure 41 also shows that there doesn't appear to be a size or number dependency correlating with the agreement of the different size measurements.

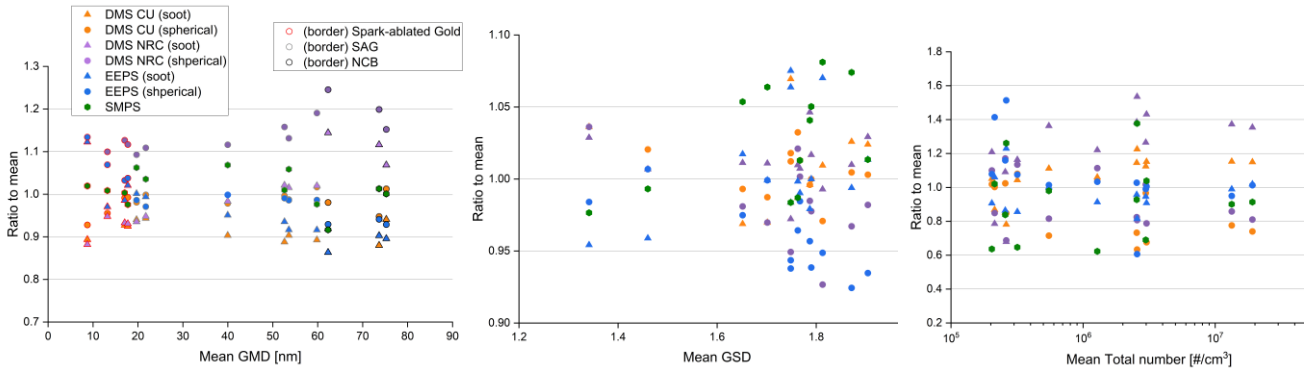

Figure 41: Ratio of individual size instruments to the mean of all instruments Vs GMD, GSD and total number for the size intercomparison experiment

Regarding the DMS500 and EEPS inversion matrices, they are seen to significantly impact the output size distributions, with the spherical inversion generally resulting in a larger GMD and smaller total number for the DMS500 (trends not as consistent with the EEPS). For information, the calibration procedure for the EEPS and DMS500 are not identical, with the most notable differences being the source used for the soot inversion (diesel engine for EEPS and Mini-CAST generator for DMS500) and the fact that the EEPS is calibrated against a DMA-CPC when the DMS500 is calibrated against a DMA-electrometer. Details of the calibration aerosols used by TSI and Cambustion are listed below.

EEPS calibration procedure[16,17&18]:

- **Spherical (i.e., compact)**:
  - <30 nm: sucrose and PAO oil generated from an electrospray aerosol generator
  - 30-560 nm: NaCl and PAO oil generated from a collision-type atomiser
- **Soot**:
  - Diluted diesel engine exhaust

DMS calibration procedure[19] :

- **Spherical**:
  - 15 nm: Sulphuric acid generated from a collision-type atomiser
  - 50 & 100 nm: NaCl generated from a collision-type atomiser
- **Soot**:
  - 50 - 300 nm: Soot from Jing Mini-Cast generator

[16] https://tsi.com/getmedia/22bf0106-13d9-4503-b179-bc76cb55e100/Updated_Inversion_Matrices_EEPS-005-A4-web?ext=.pdf
[17] https://tsi.com/getmedia/9198333e-9bce-44bf-ae55-0041311f1555/Summary_Inversion_Matrices_App_Note_EEPS-006_A4-web?ext=.pdf
[18] Wang et al. (2016) Improvement of Engine Exhaust Particle Sizer (EEPS) size distribution measurement – I&II. Engine exhaust particles Journal of Aerosol Science Volume 92, February 2016, Pages 83-108
[19] https://www.datocms-assets.com/29100/1608723874-dms-calibration-v3.pdf

5.6.2. Measured particle size distributions

To provide visualisation of the actual size distributions reported by the respective size analysers in the generation of the data presented in Section 5.6, the discreet inverted spectra from the EEPS (soot & spherical) and DMS (soot & spherical) and the reported distribution from the SMPS are presented for the VSParticle generated SAG and spark ablated gold and for non-hydrogenated NCB in Figure 42.

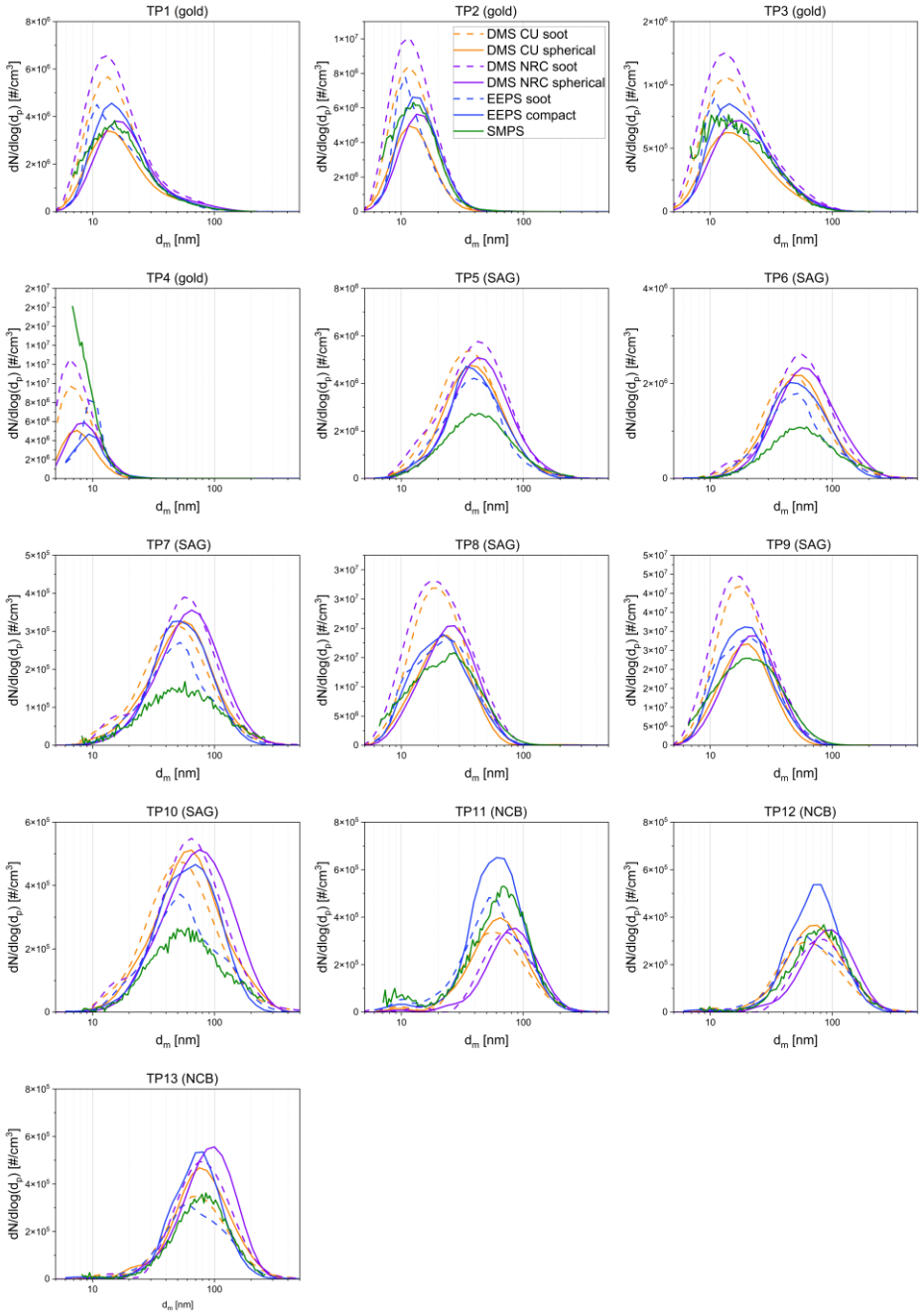

Figure 42: Measured particle size distributions during size intercomparison experiment using Spark Ablated Gold and Spark Ablated Graphite (SAG) and using non-hydrogenated Nebulised Carbon Black (NCB)

As can be seen even though the GMD and GSD were shown to be largely in agreement in Table 5 the actual spectra for a given condition and aerosol type highlights that the measured distributions show differences in the measured shape and number concentrations. This is particularly prominent in the case of the small spark ablated gold (TP4), with the SMPS not resolving the lower size range of the curve. Similarly for the SAG (TP8&9)

it is observed that the SMPS and EEPs appear to see a bimodality in the distribution which is not witnessed in the DMS500 with the soot inversion.

5.6.3. Effect of hydrogenating NCB on size analysers charging efficiency

The effect of hydrogenating NCB (i.e., exposing the carbon black powder to a hydrogen rich atmosphere, in a furnace, in an attempt to remove bound oxygen) on the charging state of the suspension was investigated by comparing the particle size distributions measuring hydrogenated NCB with and without an in-line soft-Xray source, with the results shown in Figure 43.

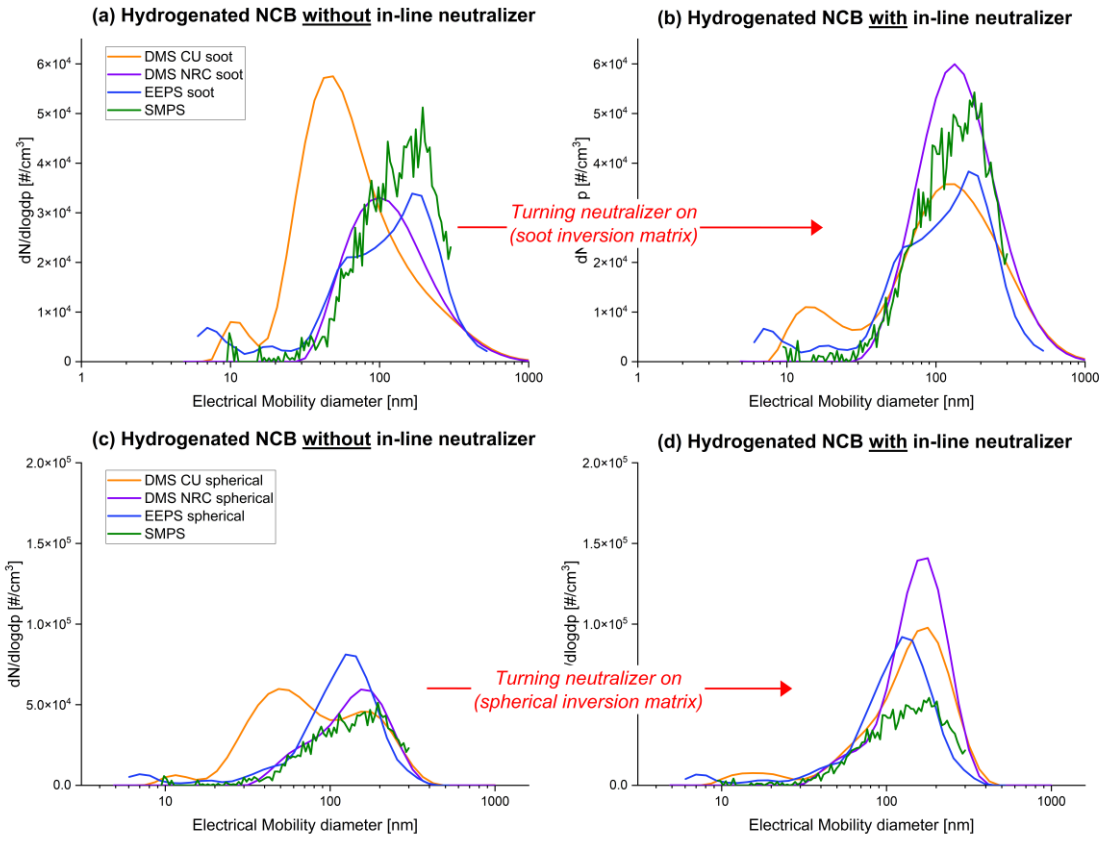

Figure 43: Particle size distributions of hydrogenated NCB with and without an additional neutraliser using various sizing analysers and inversion matrices

As can be seen, it is apparent that the CU DMS500 is impacted by a change in surface charge, given with the X-ray neutraliser powered on (Figure 43 b & d), the GMD increases by ~ 40 nm and a multimodal distribution for the case of both the soot and spherical inversion matrix when compared with the X-ray neutraliser powered off (Figure 43 a & c). Having the X-ray neutraliser on also had a significant impact on the NRC DMS500 with a GMD increase of ~20 nm and a total number increase by a factor of two. The impact of the neutraliser on the EEPS and SMPS was less apparent, with only a total number increase of ~10% for both analysers.

These findings suggest that the DMS500 is more sensitive to potentially highly charged particles, probably because of the use of a single unipolar charger when compared with the EEPS (dual unipolar charger) and SMPS (radioactive bipolar charger). These findings also highlight that the real-time sizing instruments may experience currently unquantified additional uncertainty introduced by aerosols with highly variable charge. Currently given the sizing instruments are typically behind the ~35m long earthed sampling systems and aircraft soot is assumed to have negligible charge potential this may not cause any issue. However, this suggests that further understanding of the charge potential of aircraft emissions is required, particularly if there is the potential for sizing instruments to be used on simplified (short) sampling systems in the future.

6. Particle size measurements from 'novel' calibration suspensions (SiO_2, Gold & Aircraft soot)

6.1. Suspensions as calibration checks for SMPS (SiO_2 & Gold)

Currently, generally only NIST traceable Polystyrene Latex (PSL) spheres are used for calibration checks of SMPS. However, PSL can only be used down to ~100 nm because they require a surfactant to prevent agglomeration in their suspension which results in an interfering residual peak < 100 nm.

However, building on previous studies[20], two other traceable solid spherical particles in suspensions, namely ~15 nm gold[21] (and ~ 20 nm silica[22] were investigated with the hypothesis that they didn't require a surfactant and therefore would be measurable at sizes <100nm.

SMPS scans are shown in Figure 44 highlighting that both the nebulised silica and nebulised gold peaks are clearly seen (as indicated in dashed circle). However, a significant residual peak is still present > 20 nm. This non silica/gold contamination residual peak resulted in difficulties for the DMS500 and EEPS being able to resolve the Gold/Silica peaks due to the instruments having lower particle size resolution compared to SMPS as seen in Figure 45. It is noted that there is currently an approximate 7 nm offset for both materials to the reported mobility size but the SMPS although normalised, had not been size shifted to the PSL spheres during the pre-check.

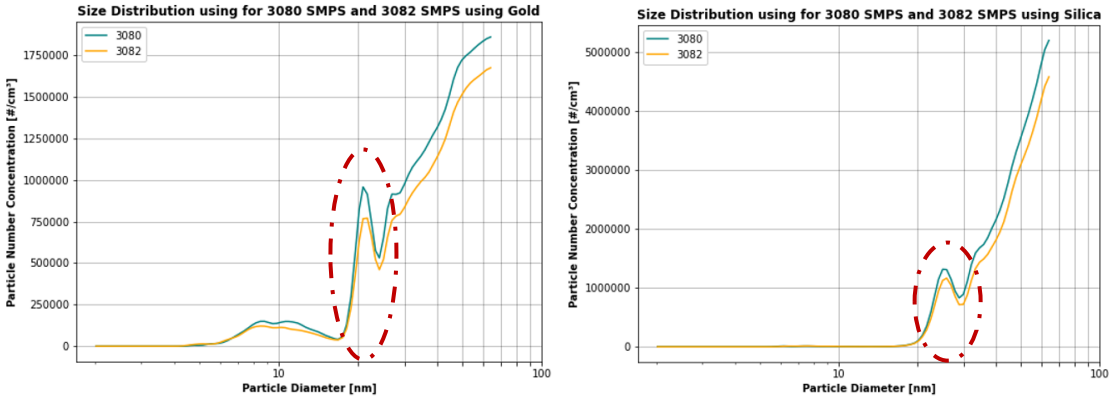

Figure 44: Nebulised 15 nm (by electron microscopy) gold suspension (left) and 20 nm (by electron microscopy) SiO_2 suspension (right) measured by a SMPS

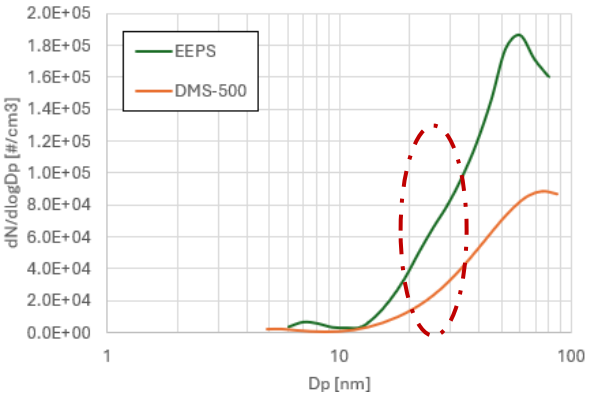

Figure 45: Nebulised 20 nm (by electron microscopy) SiO2 suspension measured by a DMS500 and EEPS

[20] Durand 'Towards improved correction methodology for regulatory aircraft engine nvPM measurement.' PhD Thesis Cardiff University (2019) - https://orca.cardiff.ac.uk/id/eprint/126400/

[21] https://nanocomposix.com/products/econix-gold-nanospheres-pvp?_pos=6&_sid=19693d701&_ss=r&variant=15906926788697

[22] https://nanocomposix.com/collections/silica-nanoparticles?variant=15906837954649

6.2.Suspended aircraft soot for in-field checks

In addition to suspending traceable Carbon Black in water for nebulisation (NCB), as was used in the size and mass instrument intercomparisons, CU used the same method to suspend aircraft soot, collected from the exit nozzle of a PW4000 engine by ZHAW, in water which could then be nebulised to create an aerosol of aviation soot (NAS). Due to the small volumes of sample collected, unfortunately it was only possible to produce 100 µg/ml in suspension, which is 10 times more dilute than the NCB solutions formulated for this study. However, when the PW4000 suspension was nebulised (NAS_{PW4000}), this soot was seen to be measurable resulting in the size distributions shown in Figure 46.

It is seen that a mode is witnessed at ~ 60 nm for NAS_{Pw4000}, which appears similar to the peak witnessed in the case of non-hydrogenated NCB. However, as would be expected due to the order of magnitude lower mass concentration, this peak is relatively lower with the 'residual peak' seen at 12nm dominating the distribution as is the case for the 1µg/ml NCB solution. It is currently unknown why there appears to be a higher residual peak in the case of the collected aircraft soot (NAS_{PW4000}). With it hypothesised this may be a result of contaminants in either the water or on the collected soot, or potentially an artifact of the actual soot collection with small soot particles being present in the aerosol. It may also be that the higher concentration of large particles for the 1 mg/mL NCB suspension is more effective at 'scavenging' the residuals (i.e. the residuals are deposited on the NCB particles instead of remaining as independent particles in the suspension).

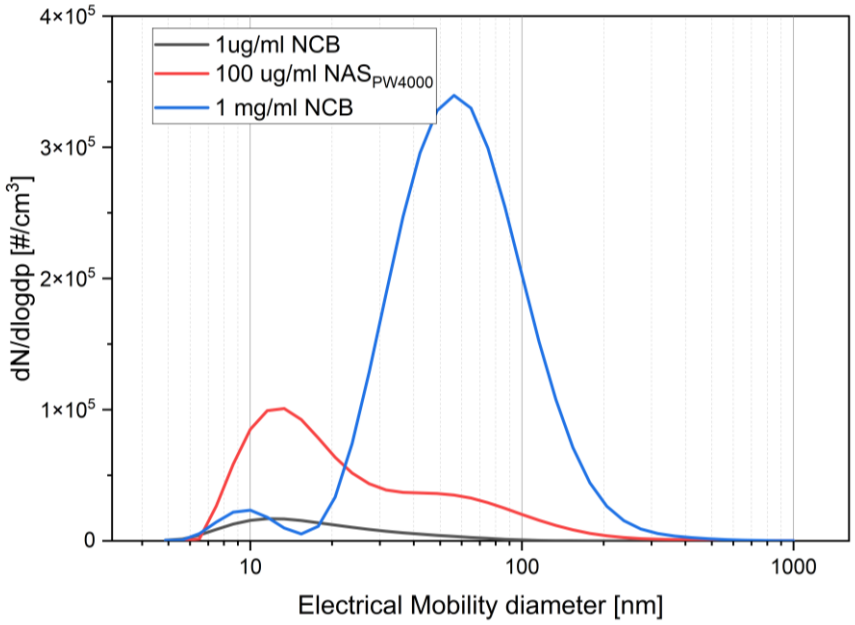

Figure 46: Particle size distributions of non-hydrogenated suspensions of Nebulised Carbon Black (NCB) and Nebulised Aircraft Soot (NAS_{PW4000}) using a DMS500

As a proof of concept this offers a potential opportunity, for the aeronautical research community, as it may be assumed that the collected soot from actual aircraft exhaust will have material properties most similar to those witnessed in real aircraft exhaust. As such, this line of study warrants further investigation towards developing methodology for collection of 'real' aircraft soot and suspending this in water for on-field checks and potentially even calibration of mass, number, and sizing instruments.

7. Particle charge investigation

The UDAC is a Unipolar Diffusion Aerosol Charger which unlike a traditional X-ray or Kr-85 aerosol neutraliser, puts a high concentration of either positive or negative charges on particles. The principle of operation is based on corona discharge, the same as the charger in the Cambustion DMS500. Traditional chargers (neutralisers) produce a significant fraction of uncharged particles, which means the counting statistics of SMPS particle size distributions measurements are poor.

These experiments looked at the effect of using a UDAC by scanning the output from two particle sources (SPG generated silver and VSParticle SAG) with two SMPS: a 3080 with a Kr-85 neutraliser and a 3082 with no neutraliser. The goal was to assess if the UDAC could be used to improve counting statistics which would benefit calibrations and line loss validations. A schematic of the setup used to investigate particle charge is shown in Figure 47.

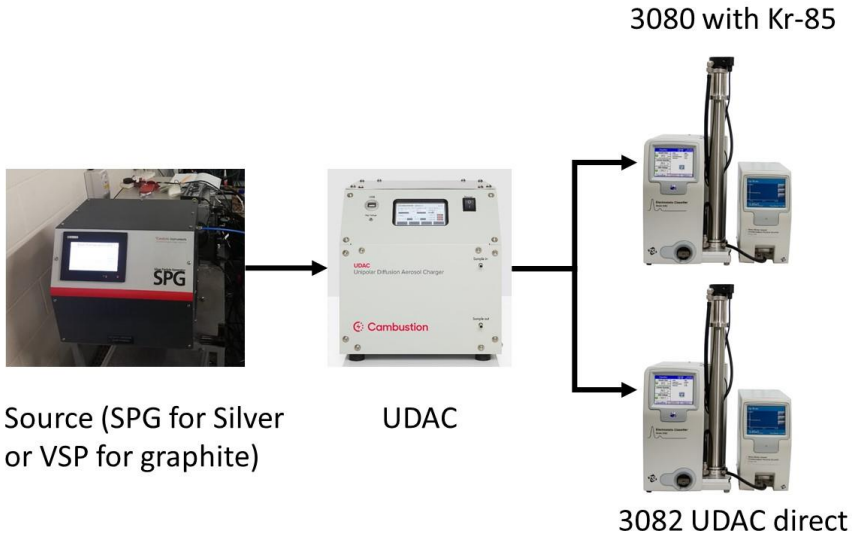

Figure 47: Schematic of experimental Set-up used to assess particle charge

It is important to note that because the particles as measured by the SMPS 3082 have an unknown number of charges per particle, direct comparison of number and size is not possible – only relative number concentrations. Furthermore, If the UDAC puts more charge on a particle than a standard neutraliser, the SMPS 3082 software inversion will “calculate” the particle to be smaller.

In these experiments, the UDAC was used to charge particles from two different sources. Firstly, SPG silver particles (Catalytic Instruments). Secondly, SAG particles (VSParticle). The SPG produced particles less than 10nm in diameter, whereas the VSParticle generally produced particles greater than 10nm.

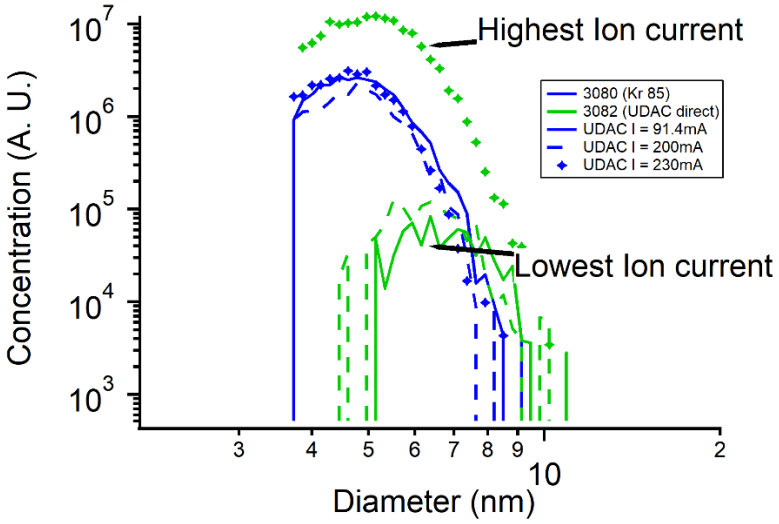

Figure 48: Comparison of two SMPS on SPG generated Silver Particles

Figure 48 shows the comparison of the two SMPS on the SPG for the smallest generated silver particles. The number of particles as seen by the SMPS 3082 increases with increasing ion current. Higher ion currents produce more ions in the corona and therefore charges more of the silver particles. The particles may have only 1 charge from the UDAC as the modes are similar at high ion currents. This suggests that using the UDAC at high ion current might improve counting statistics across the particle size distribution. Potentially this could significantly improve counting the smallest particles (the hardest to measure).

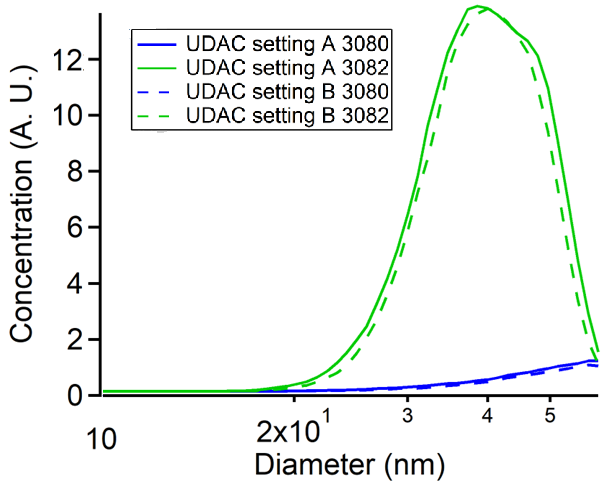

Figure 49: Comparison of two SMPS on VSParticle generated Graphite Particles

Figure 49 shows the comparison on the SAG. Although the particle distributions look different, they are physically the same particles. The UDAC direct measurement (SMPS 3082) appears to see more particles at smaller sizes. This suggests there are multiple charges on these particles and there might be higher particle numbers. This shows the potential for improving counting statistics. However, this multiple charging effect was not seen on the SPG silver particles, and it is unknown whether this was due to the different particle composition.

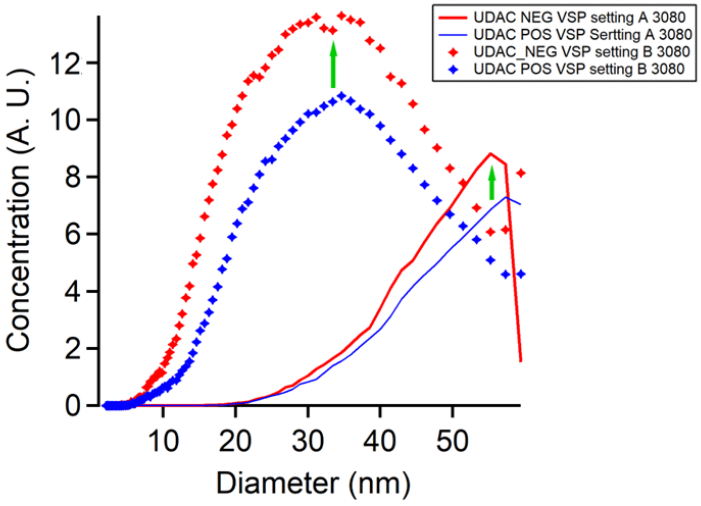

Figure 50: SMPS scan of UDAC when switched from positive to negative mode

Figure 50 shows the SMPS 3080 scanning the output of the UDAC when it is switched between positive and negative mode from the VSParticle generator. The SMPS 3080 has the Kr-85 neutraliser, so it may be assumed that these distributions are not an artefact of highly charged particles. This shows that the pre-charged state does impact the distribution measured by the SMPS. Negatively charged particles from the UDAC consistently produced higher total number when inverted by the 3080 after the Kr-85 neutraliser. This does raise questions of what the charge state of an engine particle is, as this could impact any planned particle size distribution measurements closer to the engine exit. In agreement with the earlier findings concerned with hydrogenated NCB, this suggests further investigation as to the charge state of engine nvPM particles is warranted.

8. Characterisation of particle losses in Splitter 1

It was hypothesised unequal flows in Splitter 1 of a regulatory compliant sampling system could induce additional particle loss for both mass (dominated by inertial particle loss) and number (dominated by diffusional particle loss). Therefore, as part of this test programme, the impact of changing the sample flow configuration in Splitter 1 was investigated by controlling the Swiss spill valve setting while sampling at positive inlet pressure. In normal operation, the valve would be fully open, ensuring the pressure at the inlet of the diluter is near ambient, and causing a large amount of sample flow to be dumped in the spill. In this experiment, over a 20 min period where the combustion rig settings were kept constant, the spill valve setting was changed from fully open to fully closed, reducing the flowrate in the spill (i.e., the flow configuration in splitter 1) and increasing the pressure at the inlet of the diluter.

The impact of the Swiss spill setting was first assessed on the EUR nvPM analysers. As can be seen in Figure 51, for the range of available settings and flow (which was less than can be observed on engine sample rakes) there is no correlation between the Swiss spill setting and the DF1 corrected mass and number, with fluctuations between test points attributed to rig fluctuation over the 20 minute period given both number and mass followed the same trends, regardless of the spill being open or closed.

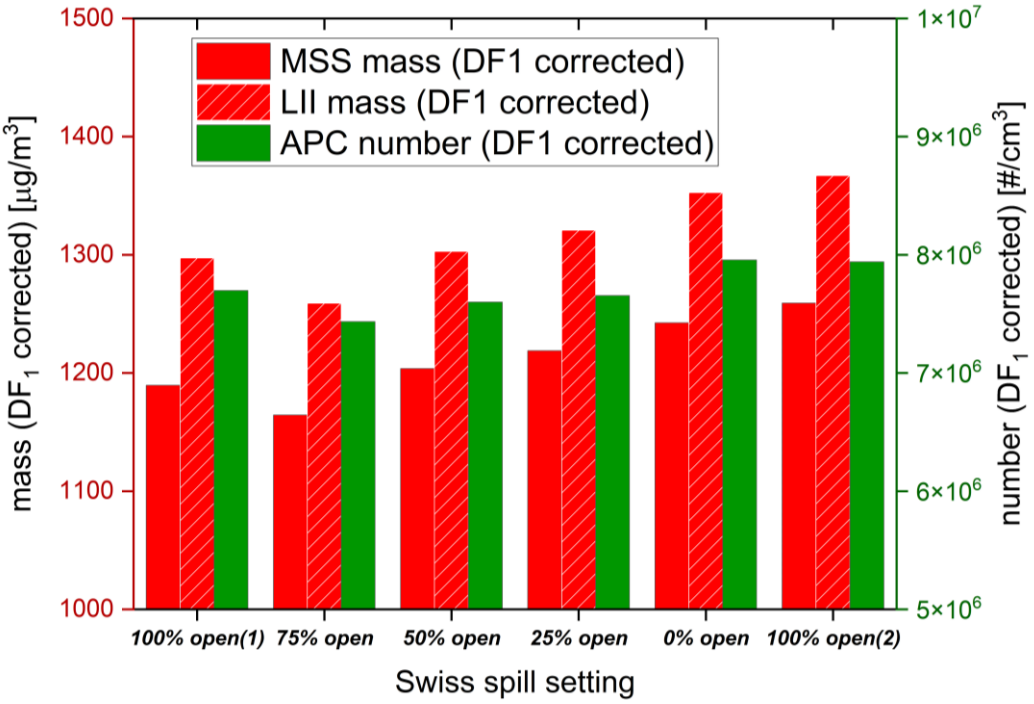

Figure 51: CU mass (MSS, LII-300) and number (APC) variation when Swiss opening/closing their spill

The impact of the spill valve opening on the relative agreement of the Emission Indices determined using the two systems is shown in Figure 52. At fully open, the P_1 pressure in the Swiss system was ~1013 mbar. At fully closed, the pressure was ~1050 mbar (+37 mbar). No significant trend could be observed as a function of the spill opening. The variability in the relative agreement between the two systems could be attributed to the fluctuation of the RQL rig (including mass to number ratio). Note that depending on a specific engine probe/rake design, the diluter inlet pressure with the spill closed can be significantly higher than +37 mbar (>100 mbar) creating larger spill/sample flow ratios than were possible for this experiment.

A more stable particle source with a system capable of simulating a full range of split velocities is ideally needed to fully assess the impact of unequal flow splitting.

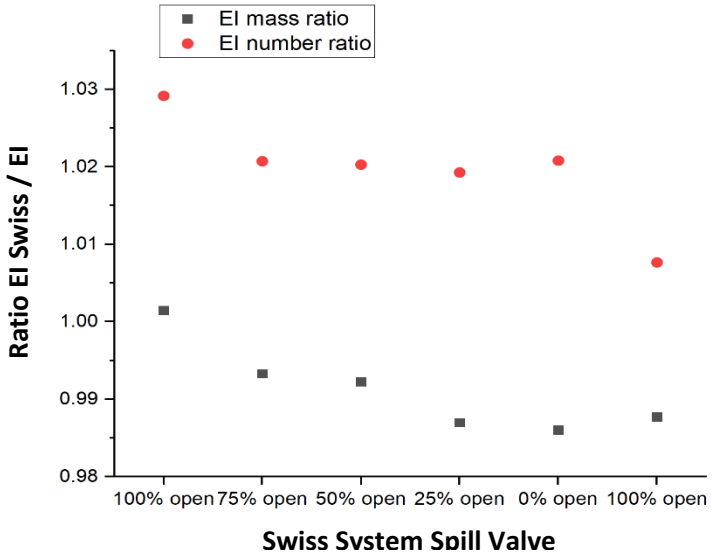

Figure 52: Ratio of the Emission Indices determined using the Swiss and EUR systems as a function of the spill opening in the Swiss system.

APPENDIX

Dry Block Calibration Certificate – used for EUR & Swiss T_1 experiments

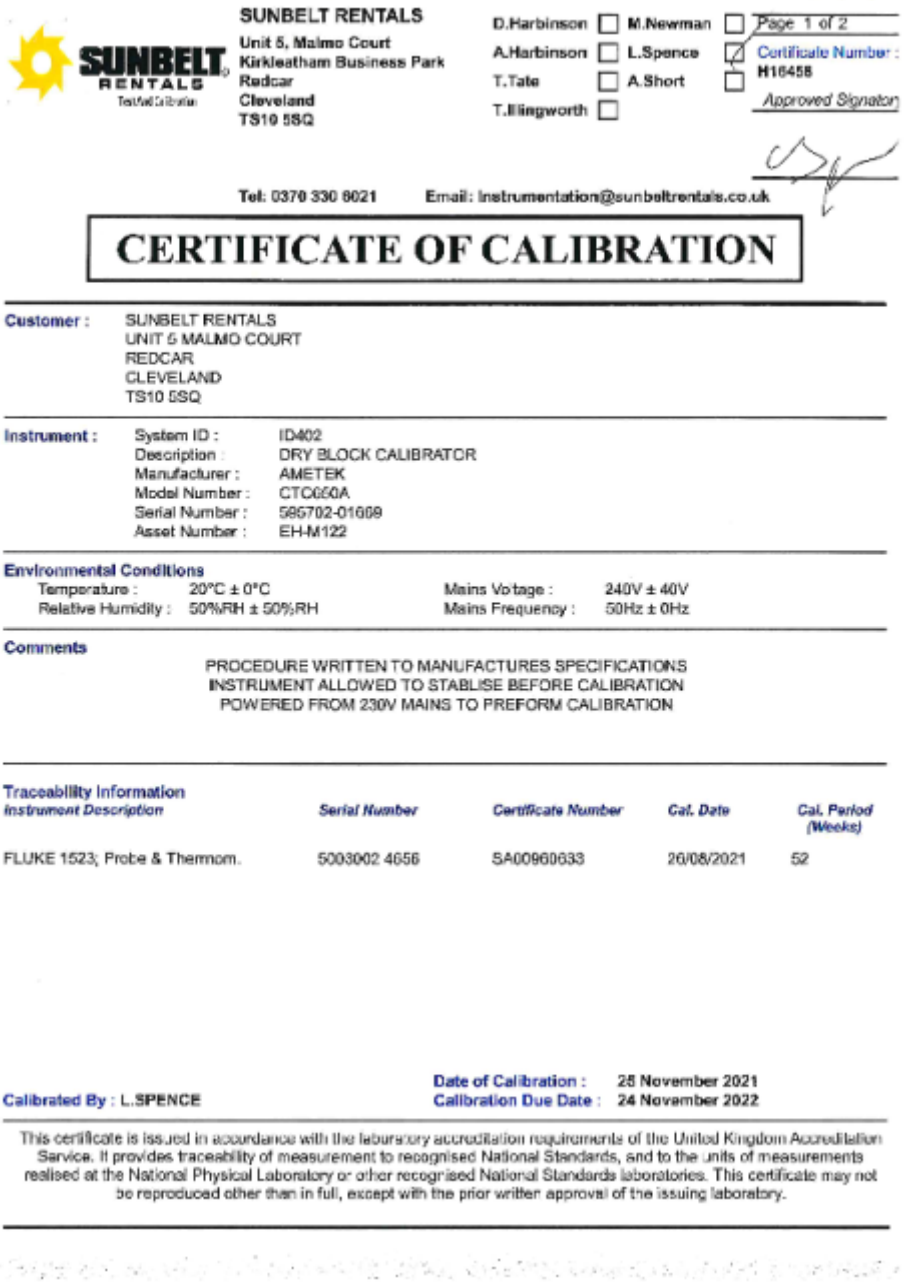

SUNBELT RENTALS
Unit 5, Malmo Court
Kirkleatham Business Park
Redcar
Cleveland
TS10 5SQ

D.Harbinson ☐ M.Newman ☐
A.Harbinson ☐ L.Spence ☑
T.Tate ☐ A.Short ☐
T.Ellingworth ☐

Page 1 of 2
Certificate Number : H16458
Approved Signator

Tel: 0370 330 6021 Email: Instrumentation@sunbeltrentals.co.uk

CERTIFICATE OF CALIBRATION

Customer : SUNBELT RENTALS
UNIT 5 MALMO COURT
REDCAR
CLEVELAND
TS10 5SQ

Instrument :

System ID :	ID402
Description :	DRY BLOCK CALIBRATOR
Manufacturer :	AMETEK
Model Number :	CTC650A
Serial Number :	585702-01609
Asset Number :	EH-M122

Environmental Conditions

Temperature :	20°C ± 0°C	Mains Voltage :	240V ± 40V
Relative Humidity :	50%RH ± 50%RH	Mains Frequency :	50Hz ± 0Hz

Comments

PROCEDURE WRITTEN TO MANUFACTURES SPECIFICATIONS
INSTRUMENT ALLOWED TO STABLISE BEFORE CALIBRATION
POWERED FROM 230V MAINS TO PREFORM CALIBRATION

Traceability Information

Instrument Description	Serial Number	Certificate Number	Cal. Date	Cal. Period (Weeks)
FLUKE 1523; Probe & Thermom.	5003002 4656	SA00960633	26/08/2021	52

Calibrated By : L.SPENCE

Date of Calibration : 25 November 2021
Calibration Due Date : 24 November 2022

This certificate is issued in accordance with the laboratory accreditation requirements of the United Kingdom Accreditation Service. It provides traceability of measurement to recognised National Standards, and to the units of measurements realised at the National Physical Laboratory or other recognised National Standards laboratories. This certificate may not be reproduced other than in full, except with the prior written approval of the issuing laboratory.

Rolls-Royce T_1 temperature lab experiment data validation

Thermocouple signals were simulated using a Druck DPI620, serial number 02918726, calibration 0087500. Thermocouples were connected using a TC-2905 (Serial Number 114CC4D) connected to a SCXI-1102 (serial number 1A8BF6D, calibration 382460-01). All inputs on the TC-2905 were set to ground reference and the pull-up resistor for open circuit detection was disabled. The SCXI-1102 inputs are set to a range of 700µV to 9000µV. The data was sampled at 1000Hz, 1000 samples are averaged every second and the results logged at 1Hz.

Raw and processed data:

• Thermocouple ID [µV] - The thermocouple voltage as read by the SCXI-1102

• Cold Junction [ºC] – The temperature of the cold junction thermistor, located in the TC-2905

• Thermocouple ID [ºC] (NIST) – Thermocouple temperatures converted using the TC-2905 cold junction thermistor and the polynomial coefficients for a K Type Thermocouple used by LabVIEW 2013 (NI documentation references NIST as the source of these coefficients).

The table below provides the response of all 11 data acquisition channels when provided with a simulated signal from the Druck. Measured temperatures have been calculated using Type K thermocouple polynomial coefficients.

Thermocouple Channel	Simulated Temperature [°C]	Mean Temperature [ºC]	Temperature Standard Deviation [ºC]
TS1	20	20.2869	0.0230
	100	100.244	0.0297
	200	200.246	0.0224
TS2	20	20.264	0.0257
	100	100.244	0.0292
	200	200.267	0.0274
TS3	20	20.2695	0.0322
	100	100.085	0.0279
	200	200.028	0.0341
TS4	20	20.0603	0.0268
	100	100.093	0.0296
	200	200.16	0.0327
TS5	20	19.9605	0.029
	100	99.834	0.0281
	200	199.799	0.0285
TS6	20	19.8174	0.0277
	100	99.782	0.0316
	200	199.823	0.0245
TS7	20	19.577	0.0386
	100	99.635	0.026
	200	199.517	0.0310
TS8	20	19.6182	0.0252
	100	99.6	0.0216
	200	199.613	0.0286
TS9	20	19.78	0.026
	100	99.696	0.0312
	200	199.69	0.0328
TS10	20	19.7958	0.0313
	100	99.763	0.0306
	200	199.804	0.0307
TS11	20	19.816	0.037
	100	99.75	0.0235
	200	199.728	0.0264

AVL 489 Particle Counter Aviation Calibration Certificate

Date:	30-Sep-2020
Device: GH0965	382
Chopper Diluter	460

Makro	XF0339	V1.30

Used Instruments	Type	Serial No.
DMA	TSI 3080	71124079
Master CPC	TSI TSI 3772	3772121004
Mass Flow Meter	Vögtlin GCR-B5SA-BA25	141570
Calibration aerosol: APG combustion soot		

Measured Inlet Flows of Instruments		
Device	Vol. Flow	Normalization Cond.
APC Chopper Dil. low	4791 ml/min	25°C; 1013.25mbar
Master CPC	1021 ml/min	ambient conditons

Zero Concentration with HEPA-Filter		
APC	0.29 #/cm³	at pcrf=10*10=100
Master CPC	0.000 #/cm³	

Nr	values set: Diluter 1 low/high	Diluter 1	Diluter 2	set pcrf	Flows: Dilution Factor	Measured Penetrations: 100nm (>70%)	50nm (>65%)	30nm (>55%)	15nm (>30%)
1	low	10	10	**100**	**73**	76.3%	72.9%	68.8%	51.4%
2	low	25	10	**250**	**187**	77.6%	76.3%	70.5%	50.4%
3	low	50	10	**500**	**376**	79.0%	77.0%	70.8%	50.6%
4	low	100	10	**1000**	**762**	81.2%	78.5%	69.8%	49.9%
5	low	150	10	**1500**	**1153**	84.0%	77.5%	70.5%	47.2%

***Only calibrated at Stages 1-5. One of those stages MUST be used for ICAO Annex 16: Environmental Protection, Vol. II, Appendix 7 compliant measurements.**

Volatile Particle Removal Efficiency for Tetracontane 30nm:	**99.76%**

AVL List GmbH does hereby certify that the above described instrument conforms to the original manufacturer's specifications and has been calibrated using standards whose accuracies are traceable to national standards or have been derived from accepted values of natural physical constants or have been derived by the ration type of self calibration techniques. This report may not be reproduced, except in full, unless permission for the publication of an approved abstract is obtained in writing from the calibration organization issuing this report.

Signature
(Armin Sejdic)

Kalibrierung - Zähleffizienz - **außerhalb des akkreditierten Partikelgrößenbereichs**
*Calibration - Counting efficiency - **not within the accredited particle size range***

Partikelgröße* *Particle size** [nm]	Nom. konzentration *Nom. concentration* [#/cm³]	Gem. Konzentration *Meas. Concentration* [#/cm³]	Referenzkonz. *Reference conc.* [#/cm³]	Zähleffizienz *Counting eff.* []	rel. Messunsicherheit *rel. meas. uncertainty* []
15	7000	6318	*7034*	*0.898*	*5.9%*
10	3000	2395	*3192*	*0.750*	*7.9%*

* Die Messunsicherheit für die Partikelgröße beträgt 4% laut Kalibrierung des DEMC bei einem Nationalen Metrologischen Institut.
* *The measurement uncertainty for the particle size is 4% according to the calibration of the DEMC at a National Metrological Institute.*

Evaluierung* der Limits entsprechend UN/ECE GRPE-PMP Sub23nm draft
Limit evaluation according UN/ECE GRPE-PMP Sub23nm draft*

Kalibrierung - Linearität
Calibration - Linearity

Nr. *No.*	Nom. Konz. *Nom. Conc.* [#/cm³]	Ref. Konz. *Ref. Conc* [#/cm³]	Gem. Konz. *Meas. Conc.* [#/cm³]	Zähleffizienz *Counting eff.* []	Limit *Limit* []	Status *Status* []	Residuum abw. *Residual dev.* [%]
1	10000	9375	9081	*0.969*	0.9-1.1	*passed*	*0.3%*
2	8000	7765	7504	*0.966*	0.9-1.1	*passed*	*0.1%*
3	6000	5907	5663	*0.959*	0.9-1.1	*passed*	*-0.7%*
4	4000	4117	3954	*0.960*	0.9-1.1	*passed*	*-0.5%*
5	2500	2569	2462	*0.958*	0.9-1.1	*passed*	*-0.7%*
6	0	0	0	-	<0.5#/cm³	*passed*	-

Berechnung des k-Faktors bei 55nm
k-factor calculation at 55nm

	Wert *Value*	Limit *Limit*
Steigung/Slope	0.965	0.9-1.1
R^2	1.000	>0.97
k-Faktor	1.036	-

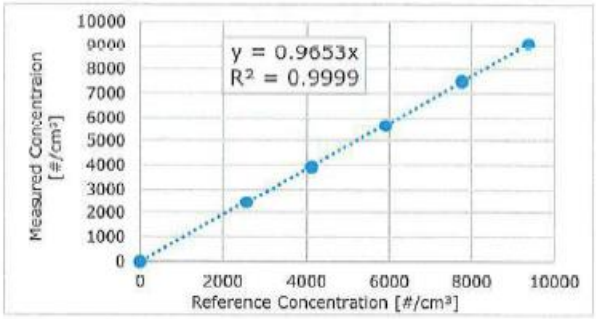

Zähleffizienz bei 10nm und 15nm mit angewandtem k-Faktor
Counting efficiency at 10nm and 15nm with k-factor applied

Partikelgröße *Particle size* [nm]	Zähleffizienz *Counting eff.* []	Limit *Limit* []	Status *Status* []
10	0.777	0.5-0.8	*passed*
15	0.930	≥0.9	*passed*

AVL 489 Particle Counter Aviation Calibration Certificate

Date:	29-Sep-2020	
Device:	GH0672	409
	Chopper Diluter	507

Makro	XF0339	V1.30

Used Instruments	Type	Serial No.
DMA	TSI 3080	71124079
Master CPC	TSI TSI 3772	3772121004
Mass Flow Meter	Vögtlin GCR-B5SA-BA25	141570
Calibration aerosol: APG combustion soot		

Measured Inlet Flows of Instruments		
Device	Vol. Flow	Normalization Cond.
APC Chopper Dil. low	4376 ml/min	25°C; 1013.25mbar
Master CPC	1010 ml/min	ambient conditons

Zero Concentration with HEPA-Filter		
APC	0.04 #/cm³	at pcrf=10*10=100
Master CPC	0.000 #/cm³	

Nr	values set: Diluter 1 low/high	Diluter 1	Diluter 2	set pcrf	Flows: Dilution Factor	Measured Penetrations: 100nm (>70%)	50nm (>65%)	30nm (>55%)	15nm (>30%)
1	low	10	10	**100**	**71**	73.9%	72.4%	67.7%	48.4%
2	low	25	10	**250**	**179**	76.2%	72.7%	67.3%	47.0%
3	low	50	10	**500**	**363**	76.6%	74.1%	67.7%	47.0%
4	low	100	10	**1000**	**705**	75.3%	71.3%	65.8%	44.2%
5	low	150	10	**1500**	**1051**	73.5%	73.2%	64.0%	41.7%

***Only calibrated at Stages 1-5. One of those stages MUST be used for ICAO Annex 16: Environmental Protection, Vol. II, Appendix 7 compliant measurements.**

Volatile Particle Removal Efficiency for Tetracontane 30nm:	**99.99%**

AVL List GmbH does hereby certify that the above described instrument conforms to the original manufacturer's specifications and has been calibrated using standards whose accuracies are traceable to national standards or have been derived from accepted values of natural physical constants or have been derived by the ration type of self calibration techniques. This report may not be reproduced, except in full, unless permission for the publication of an approved abstract is obtained in writing from the calibration organization issuing this report.

Signature

(Armin Sejdic)

Kalibrierung - Zähleffizienz - **außerhalb des akkreditierten Partikelgrößenbereichs**
*Calibration - Counting efficiency - **not within the accredited particle size range***

Partikelgröße* *Particle size** [nm]	Nom. konzentration *Nom. concentration* [#/cm³]	Gem. Konzentration *Meas. Concentration* [#/cm³]	Referenzkonz. *Reference conc.* [#/cm³]	Zähleffizienz *Counting eff.* []	rel. Messunsicherheit *rel. meas. uncertainty* []
15	7000	5585	*6188*	*0.902*	*5.9%*
10	3000	2284	*3029*	*0.754*	*7.9%*

* Die Messunsicherheit für die Partikelgröße beträgt 4% laut Kalibrierung des DEMC bei einem Nationalen Metrologischen Institut.
* *The measurement uncertainty for the particle size is 4% according to the calibration of the DEMC at a National Metrological Institute.*

Evaluierung* der Limits entsprechend UN/ECE GRPE-PMP Sub23nm draft
Limit evaluation according UN/ECE GRPE-PMP Sub23nm draft*

Kalibrierung - Linearität
Calibration - Linearity

Nr. *No.*	Nom. Konz. *Nom. Conc.* [#/cm³]	Ref. Konz. *Ref. Conc* [#/cm³]	Gem. Konz. *Meas. Conc.* [#/cm³]	Zähleffizienz *Counting eff.* []	Limit *Limit* []	Status *Status* []	Residuum abw. *Residual dev.* [%]
1	10000	9759	9241	*0.947*	0.9-1.1	*passed*	*-0.5%*
2	8000	8035	7637	*0.950*	0.9-1.1	*passed*	*-0.1%*
3	6000	6159	5916	*0.961*	0.9-1.1	*passed*	*1.0%*
4	4000	4377	4185	*0.956*	0.9-1.1	*passed*	*0.5%*
5	2500	2621	2507	*0.957*	0.9-1.1	*passed*	*0.6%*
6	0	0	0	-	<0.5#/cm³	*passed*	-

Berechnung des k-Faktors bei 55nm
k-factor calculation at 55nm

	Wert *Value*	Limit *Limit*
Steigung/Slope	0.951	0.9-1.1
R^2	1.000	>0.97
k-Faktor	1.051	-

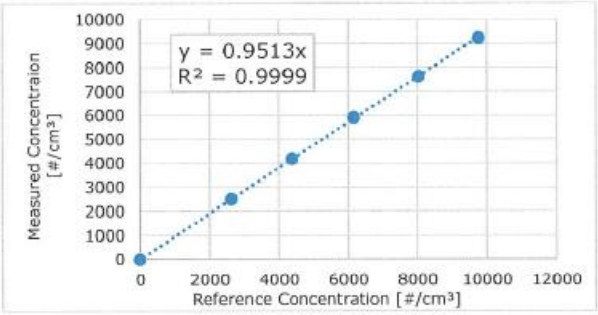

Zähleffizienz bei 10nm und 15nm mit angewandtem k-Faktor
Counting efficiency at 10nm and 15nm with k-factor applied

Partikelgröße *Particle size* [nm]	Zähleffizienz *Counting eff.* []	Limit *Limit* []	Status *Status* []
10	0.792	0.5-0.8	*passed*
15	0.949	≥0.9	*passed*

MATLAB code for the calculation of GMD, GSD and total number

```
function [results]=size_intercomparison_raptor(Dp, PSD)

A=size(PSD);
tend=A(1,1);

    for i =1:1:tend

        if PSD(i,70)==0
        else

            Ntot(i,1)=trapz(log10(Dp),PSD(i,:));

GMD(i,1)=round(10^(trapz(log10(Dp),PSD(i,:).*log10(Dp))/Ntot(i)),1);

GSD(i,1)=round(10^sqrt(trapz(log10(Dp),PSD(i,:).*log10(Dp).^2)/Ntot(i)-
log10(GMD(i)).^2),2);

            lognorm='a*exp(-0.5*((log((x)/b)/c)^2))';
            fit_logn=fit(Dp',PSD(i,:)',lognorm,'start',[
Ntot(i,1)*log(10)/(sqrt(2*pi)*log(GSD(i,1))) GMD(i,1)
log(GSD(i,1))],'lower', [0 3 log(1.2)]);
            coef_fit=coeffvalues(fit_logn);
            GMD_logn(i,1)=coef_fit(2);
            GSD_logn(i,1)=exp(coef_fit(3));
            Ntot_logn(i,1)=coef_fit(1)/log(10)*sqrt(2*pi)*log(GSD_logn(i,1));

            results(i,1)=GMD(i,1);
            results(i,2)=GSD(i,1);
            results(i,3)=Ntot(i,1);

            results(i,5)=round(GMD_logn(i,1),1);
            results(i,6)=round(GSD_logn(i,1),2);
            results(i,7)=Ntot_logn(i,1);
        end
    end

    clearvars Ntot GMD GSD lognorm fit_logn coef_fit GMD_logn GSD_logn
Ntot_logn A i

end
```

Size instrument calibration certificates

CAMBUSTION

DMS500 Certificate of Calibration with Soot Agglomerates

after Service and Adjustment

Company Name: Cardiff University	Instrument Serial №: M44
Company Location: Wales, UK	Calibration № (matrix): m2cqs663
Ship Date: September 2020	Date Calibrated: 25th September 2020

In addition to the standard spherical calibration (m2cqw663), an additional calibration is provided for measurement from highly fractal aerosols, e.g. Diesel. This applies only to the accumulation mode lognormal fit output given by the *Diesel* aerosol description file (.dmd).

The calibration standards used for these measurements are traceable to relevant international standards. The results refer to measurements made at the time of test and not to the instrument's ability to maintain calibration. *The reported measurement uncertainties are based upon a standard uncertainty multiplied by a coverage factor k = 2, which for a normal distribution provides a level of confidence of approximately 95%. The standard uncertainties are a consolidation of the uncertainty in the standard and the uncertainty in performing the measurement.*

Size and Gain: against Differential Mobility Analyser Sized Aerosol, with concentration indicated with a standard aerosol electrometer
Electrometer filter flow = 8.0 slpm

Aerosol	DMA Size (nm)	DMS Size (nm)	Electrometer Concentration (#/cc)	DMS Concentration (#/cc)
Soot	50.0 ± 5.0	49.5	27300 ± 5460	27200
Soot	100 ± 10	99.8	50600 ± 10100	50100
Soot	200 ± 20	201	10400 ± 2080	10300

Standards used:

Function		Mfr and Model	Serial Number	Calibrated By	Calibration Reference	Calibration Date	Calibration Due
DMA		TSI 3082	3082001529001	Cambustion	3082001529001/2020	25/08/2020	25/08/2021
Aerosol Electrometer	Electrometer	Keithley 617	425680	Trescal	41386	23/05/2020	23/05/2021
	Mass flow meter	Aalborg GFC17	224526-1	Aalborg	200406224526-1	06/04/2020	06/04/2021

Calibrator: Thomas Pim

Approved By:

Dr J.P.R. Symonds

Director

CAMBUSTION LTD

J6 The Paddocks
347 Cherry Hinton Road
Cambridge CB1 8DH
United Kingdom
Tel: +44 1223 210250
Fax: +44 1223 210190
E-mail: *cambustion@cambustion.com*

DMS500 Certificate of Calibration

after Service and Adjustment

Company Name: Cardiff University	Instrument Serial №: M44
Company Location: Wales, UK	Calibration № (matrix):m2cqw663
Ship Date: September 2020	Date Calibrated: 25th September 2020

The DMS500 system is certified as meeting or exceeding the Test Specifications, when tested prior to dispatch. The calibration standards used for these measurements are traceable to relevant international standards. The results refer to measurements made at the time of test and not to the instrument's ability to maintain calibration. *The reported measurement uncertainties are based upon a standard uncertainty multiplied by a coverage factor k = 2, which for a normal distribution provides a level of confidence of approximately 95%. The standard uncertainties are a consolidation of the uncertainty in the standard and the uncertainty in performing the measurement.*

(a) Size and Gain: against Differential Mobility Analyser Sized Aerosol, with concentration indicated with a standard aerosol electrometer
Electrometer filter flow = 8.0 slpm

Aerosol	DMA Size (nm)	DMS Size (nm)	Electrometer Concentration (#/cc)	DMS Concentration (#/cc)
H_2SO_4	15.0 ± 1.5	15.1	117000 ± 23500	118000
NaCl	50.0 ± 5.0	50.3	131000 ± 26100	133000
NaCl	100 ± 10	101	36800 ± 7360	36400

(b) Size Only: Nebulised, dried and neutralised suspension of NIST Traceable Certified NanoSpheres (PSL), Thermo Scientific

PSL Size (nm)	DMS Size (nm)	Lot No	Expiry Date
303 ± 30	299	211102	01/05/2022
600 ± 60	596	221251	01/01/2023
903 ± 90	940	218704	01/11/2022

Standards used for part (a)

Function		Mfr and Model	Serial Number	Calibrated By	Calibration Reference	Calibration Date	Calibration Due
DMA		TSI 3082	3082001529001	Cambustion	3082001529001/2020	25/08/2020	25/08/2021
Aerosol Electrometer	Electrometer	Keithley 617	425680	Trescal	41386	23/05/2020	23/05/2021
	Mass flow meter	Aalborg GFC17	224526-1	Aalborg	200406224526-1	06/04/2020	06/04/2021

Calibrator: Thomas Pim

Approved By:

Dr J.P.R. Symonds

Director

CAMBUSTION LTD

J6 The Paddocks
347 Cherry Hinton Road
Cambridge CB1 8DH
United Kingdom
Tel: +44 1223 210250
Fax: +44 1223 210190
E-mail: *cambustion@cambustion.com*

Cambustion

DMS500 Certificate of Calibration

after Service and Adjustment

Company Name: NRC	Instrument Serial №: M125
Company Location: Canada	Calibration № (matrix):m2cqw747
Ship Date: October 2021	Date Calibrated: 8th October 2021

The DMS500 system is certified as meeting or exceeding the Test Specifications, when tested prior to dispatch. The calibration standards used for these measurements are traceable to relevant international standards. The results refer to measurements made at the time of test and not to the instrument's ability to maintain calibration. *The reported measurement uncertainties are based upon a standard uncertainty multiplied by a coverage factor k = 2, which for a normal distribution provides a level of confidence of approximately 95%. The standard uncertainties are a consolidation of the uncertainty in the standard and the uncertainty in performing the measurement.*

(a) Size and Gain: against Differential Mobility Analyser Sized Aerosol, with concentration indicated with a standard aerosol electrometer
Electrometer filter flow = 8.0 slpm

Aerosol	DMA Size (nm)	DMS Size (nm)	Electrometer Concentration (#/cc)	DMS Concentration (#/cc)
H_2SO_4	15.0 ± 1.5	15.1	43200 ± 8630	41400
NaCl	50.0 ± 5.0	49.9	31100 ± 6220	30300
NaCl	100 ± 10	102	20400 ± 4070	20500

(b) Size Only: Nebulised, dried and neutralised suspension of NIST Traceable Certified NanoSpheres (PSL), Thermo Scientific

PSL Size (nm)	DMS Size (nm)	Lot No	Expiry Date
303 ± 30	306	238629	01/03/2024
600 ± 60	602	230585	01/09/2023
903 ± 90	887	239389	01/04/2024

Standards used for part (a)

Function		Mfr and Model	Serial Number	Calibrated By	Calibration Reference	Calibration Date	Calibration Due
DMA		TSI 3082	3082001912001	Cambustion	3082001912001/2021	22/03/2021	22/03/2022
Aerosol Electrometer	Electrometer	Keithley 6514	1247513	Keithley Instruments	0500131	08/01/2021	08/01/2022
	Mass flow meter	Aalborg GFC171	224526-1	Aalborg	210524224526-1	24/05/2021	24/05/2022

Calibrator: J.Evans

Approved By: JPRS

Dr J.P.R. Symonds

Director

CAMBUSTION LTD

J6 The Paddocks
347 Cherry Hinton Road
Cambridge CB1 8DH
United Kingdom
Tel: +44 1223 210250
Fax: +44 1223 210190
E-mail: *cambustion@cambustion.com*

Cambustion

DMS500 Certificate of Calibration with Soot Agglomerates

after Service and Adjustment

Company Name: *NRC*	Instrument Serial №: M125
Company Location: Canada	Calibration № (matrix): m2cqs747
Ship Date: October 2021	Date Calibrated: *8th October 2021*

In addition to the standard spherical calibration (m2cqw747), an additional calibration is provided for measurement from highly fractal aerosols, e.g. Diesel. This applies only to the accumulation mode lognormal fit output given by the *Diesel* aerosol description file (.dmd).

The calibration standards used for these measurements are traceable to relevant international standards. The results refer to measurements made at the time of test and not to the instrument's ability to maintain calibration. *The reported measurement uncertainties are based upon a standard uncertainty multiplied by a coverage factor k = 2, which for a normal distribution provides a level of confidence of approximately 95%. The standard uncertainties are a consolidation of the uncertainty in the standard and the uncertainty in performing the measurement.*

Size and Gain: against Differential Mobility Analyser Sized Aerosol, with concentration indicated with a standard aerosol electrometer
Electrometer filter flow = 8.0 slpm

Aerosol	DMA Size (nm)	DMS Size (nm)	Electrometer Concentration (#/cc)	DMS Concentration (#/cc)
Soot	50.0 ± 5.0	49.3	17400 ± 3480	17000
Soot	100 ± 10	101	26300 ± 5270	25200
Soot	200 ± 20	204	35000 ± 7000	34000

Standards used:

Function		Mfr and Model	Serial Number	Calibrated By	Calibration Reference	Calibration Date	Calibration Due
DMA		TSI 3082	3082001912001	Cambustion	3082001912001/2021	22/03/2021	22/03/2022
Aerosol Electrometer	Electrometer	Keithley 6514	1247513	Keithley Instruments	0500131	08/01/2021	08/01/2022
	Mass flow meter	Aalborg GFC171	224526-1	Aalborg	210524224526-1	24/05/2021	24/05/2022

Calibrator: J.Evans

Approved By: JPRS

Dr J.P.R. Symonds

Director

CAMBUSTION LTD

J6 The Paddocks
347 Cherry Hinton Road
Cambridge CB1 8DH
United Kingdom
Tel: +44 1223 210250
Fax: +44 1223 210190
E-mail: *cambustion@cambustion.com*

Sample Data Sheet

Date/Time: 7/02/2020 9:11:54 AM
Instrument Label: Model 3090AK, SN: 30900196
Firmware: MCU: 3.15, DSP: 3.02

Read Status Record	Units	Nominal	3090/3091
Status Code			0x77
Error Code 1		0x0	0x0
Error Code 2		0x0	0x0
Sheath Flow	LPM	39.4±.20	39.4
Sample Flow	LPM	8.0±0.08	8.0
Charger Flow	LPM	0.60±0.02	0.6
Extraction Flow	LPM	2.00±0.02	2.0
Absolute Pressure	mBar	968±40	951.0
Voltage Top	V	85±2	85.1
Voltage Middle	V	470±10	468.7
Voltage Bottom	V	1200±4	1199.3
Sheath Flow Temp	°C	25±5	24.2
Sample Flow Temp	°C	25±5	24.2
Charger Flow Temp	°C	25±5	25.8
Extraction Flow Temp	°C	25±5	25.5
Neg. Charger Current	nA	35±0.5	34.8
Pos. Charger Current	nA	31±0.5	30.9
Neg. Charger Voltage	V	2000±500	1736.9
Pos. Charger Voltage	V	2000±500	2178.8

Zero Electrometer Table	Units	Offset Range	Offset	RMS Range	RMS
Channel 1	fA	< 750	8.6	< 15	1.2
Channel 2	fA	< 750	10.2	< 15	1.0
Channel 3	fA	< 750	10.2	< 50	2.7
Channel 4	fA	< 750	19.2	< 50	2.9
Channel 5	fA	< 750	26.9	< 50	6.5
Channel 6	fA	< 750	29.8	< 50	6.6
Channel 7	fA	< 750	28.1	< 50	3.9
Channel 8	fA	< 750	31.8	< 50	3.2
Channel 9	fA	< 750	32.5	< 50	4.3
Channel 10	fA	< 750	34.1	< 50	5.0
Channel 11	fA	< 750	61.8	< 50	10.9
Channel 12	fA	< 750	64.1	< 50	6.0
Channel 13	fA	< 750	61.2	< 50	6.2
Channel 14	fA	< 750	65.2	< 50	12.7
Channel 15	fA	< 750	61.5	< 50	3.2
Channel 16	fA	< 750	69.2	< 50	4.1
Channel 17	fA	< 750	62.9	< 50	3.9
Channel 18	fA	< 750	58.3	< 50	3.7
Channel 19	fA	< 750	61.6	< 50	6.7
Channel 20	fA	< 750	59.1	< 50	6.5
Channel 21	fA	< 750	76.1	< 50	4.5
Channel 22	fA	< 1000	56.7	< 125	5.6

External Checks	Units	Nominal	3090/91	Nominal	3090/91	Nominal	3090/91
Analog Input (Ch1)	V	1±0.5	0.99	5±0.5	4.98	9±0.5	8.95
Analog Input (Ch2)	V	1±0.5	1.00	5±0.5	4.99	9±0.5	9.00
Pump Voltages (sheath, sample, extract)	V	6.0-9.5	7.70	11.0-14.0	11.70	6.0-9.0	7.49
Check Trigger (input #1, #2, output)	V	Pass/Fail	PASS	Pass/Fail	N/A	Pass/Fail	PASS
Flow (inlet, outlet / both without cyclone)	LPM	9.6-10.2	9.87	±0.3 inlet	9.72		
Final system leak check	" h2O	< 10 per 5 min	PASS				
Heater Check (output)	A	1±0.3	1.0				

Aerosol Checkout	Units	Standard	3090/3091	% Diff	Tolerance
100nm Classified Emery Oil vs SMPS	nm	98.2	93.06	-5.2%	+/- 10% of Standard
100nm Classified Emery Oil vs CPC 3776	#/cm3	4.40E+04	4.25E+04	-3.4%	+/- 20% of Standard
Polydisperse Emery Oil vs SMPS	nm	98.2	93.06	-5.2%	+/- 10% of Standard
Polydisperse Emery Oil vs CPC 3776	#/cm3	6.63E+03	6.70E+03	1.1%	+/- 20% of Standard

Final Checkout	☑		☑
Inspect Charger Needles	YES	Hi Pot Test	YES
Add Caps to Inlet & Outlet	YES	Visual Inspect Cabinet for Blemishes	YES
Check Power Cord for Destination Country	YES	Clean & Grease Cyclone	YES

Technician: Patrick Abe

European Union Aviation Safety Agency

Konrad-Adenauer-Ufer 3
50668 Cologne
Germany

Environmental Research - Engine Emissions | EASA

Mail EASA.research@easa.europa.eu
Web www.easa.europa.eu

An Agency of the European Union